

Effects of Nonionic Surfactant Mixtures on Water Alignment at the Air-Water Interface

A Thesis Submitted in Partial Fulfillment
of the Requirements for the Degree of
Master of Science (M.Sc.) in Chemistry

Presented to the Department of Chemistry
Johannes Gutenberg University Mainz

by

Lucas Julian Gunkel

born in Lahnstein on July 7th, 1994

Period of work: 08.06.2020-11.12.2020

Prepared at: Max Planck Institute for Polymer Research
Department of Molecular Spectroscopy

Primary Reviewer **Prof. Dr. Mischa Bonn**

Secondary Reviewer **Prof. Dr. Thomas Basché**

Submitted 11.12.2020

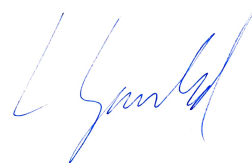
**Masterarbeit im Studiengang Chemie oder Biomedizinische Chemie
an der Johannes Gutenberg - Universität Mainz**

Ich, Lucas Gunkel, Matrikelnummer 2707210

versichere, dass ich meine Masterarbeit selbstständig verfasst und keine anderen als die angegebenen schriftlichen und elektronischen Quellen sowie andere Hilfsmittel benutzt habe. Alle Ausführungen, die anderen Schriften wörtlich oder sinngemäß entnommen wurden, habe ich kenntlich gemacht.

Mainz, 09.12.2020

(Ort, Datum)



(Unterschrift)

Abstract

Surfactants at water interfaces are of great importance to many scientific fields, such as atmospheric chemistry, biochemistry and surface science. A better understanding of the impact of surfactants on water alignment could yield further insights into biological membranes and commercially used detergents. In the past, research has been conducted on mixtures of oppositely charged surfactants, where the effects on water alignment are governed by the long range coulomb interaction aligning the molecular dipoles.

This work set out to examine the effects of charge neutral surfactant mixtures. The two simple surfactants dodecanol and dodecylamine, were selected as they only differ by their respective head group. All experiments had to be conducted at elevated pH=11, so that the amine was not protonated.

Surface pressure measurements were conducted and it was found that the surfactant mixtures show increased surface pressure compared to the neat surfactants. This was the same trend, as found for comparable ionic surfactants. This was attributed to synergistic adsorption of head-to-head complexes of the two surfactants.

For further analysis direct and phase-sensitive vibrational sum frequency generation spectroscopy (VSFG) was used. SFG is a powerful tool for probing interfaces because of the inherent selection rules stating that a SFG signal may only be generated if a vibrational mode is not centrosymmetric or in a non centrosymmetric environment.

Direct SFG revealed a similar trend for the the peak area in the bonded OH/bonded OD frequency domain to the one seen in the surface pressure measurements. The bonded OH/bonded OD peaks of the neat surfactants exhibit a higher intensity, than the surfactant mixtures. It was proposed that this may be because of different hydrogen bonding strength of the two surfactants with water, causing the surfactants to penetrate the surface to a different depth. This could disrupt the water structure at the interface causing additional disorder and therefore weaken the SFG signal.

Additionally the ratio of the CH₂ symmetric stretching (d^+) and CH₃ symmetric stretching mode (r^+) was used as an indicator for order in the monolayer. In a monolayer, where all surfactants are in an all-trans configuration, the methylene groups are in a pseudo centrosymmetric environment and therefore do not generate a SFG signal, while all methyl groups are ordered and contribute the maximum amount to the SFG signal. Therefore a high d^+ to r^+ ratio means more gauche defects and thus more disorder.

Finally phase-sensitive SFG measurements reveal a positive band centred between 2300 cm⁻¹ and 2350 cm⁻¹ in the $\text{Im}\chi^{(2)}$ spectrum. Because this band has a negative sign for neat water this positive feature is attributed to the influence of the surfactants on water alignment, and could hint on water molecules changing orientation due to hydrogen bonding with the surfactant head group.

Zusammenfassung

Tenside an Wasser-Grenzflächen sind von großer Bedeutung für viele wissenschaftliche Disziplinen wie Atmosphärenchemie, Biochemie und Oberflächenchemie. Ein besseres Verständnis des Einflusses von Tensiden auf die Ausrichtung von Wassermolekülen könnte tiefere Einblicke in biologische Membranen oder kommerzielle Detergenzien liefern. In der Vergangenheit wurden Mischungen von gegensätzlich geladenen ionischen Tensiden untersucht. Die Effekte der Tensidmischungen auf die Ausrichtung der Wassermoleküle werden durch die weitreichende Coulomb Wechselwirkung bestimmt, welche die molekularen Dipole im elektrischen Feld ausrichtet.

Diese Arbeit hat das Ziel die Effekte von nichtionischen Tensidmischungen zu untersuchen. Hierfür wurden die beiden einfachen Tenside Dodecanol und Dodecylamin ausgewählt, da sie sich nur durch ihre funktionelle Gruppe unterscheiden. Alle Experimente wurden bei erhöhtem pH-Wert (pH 11) durchgeführt, sodass Dodecylamin in der nicht protonierten Form vorliegt.

Messungen des Oberflächendruck wurden durchgeführt und es wurde herausgefunden, dass die Tensidmischungen einen erhöhten Oberflächendruck aufweisen gegenüber den reinen Tensiden. Dieser Trend ähnelt dem für vergleichbare ionische Tenside und wurde mit synergistischer Adsorption von Kopf-zu-Kopf Komplexen der beiden Tenside erklärt.

Für weiterführende Analysen wurden direkte und phasensensitive Schwingungs Summenfrequenzerzeugungs Spektroskopie (VSFG) benutzt. SFG ist ein leistungsfähiges Werkzeug für die Untersuchung von Grenzflächen, da aufgrund der inhärenten Auswahlregeln es nur zur Summenfrequenzerzeugung kommt, wenn eine Schwingungsmode nicht zentrosymmetrisch ist oder sich in einer nicht zentrosymmetrischen Umgebung befindet.

Direkte SFG enthüllte einen vergleichbaren Trend für die spektrale Fläche in der gebundenen OH/gebundenen OD Frequenzregion zu den Oberflächendruck Messungen. Die gebundenen OH/gebundenen OD Peaks der reinen Tenside zeigen ein verstärktes Signal im Vergleich zu den Tensidmischungen. Es wurde vorgeschlagen, dass die unterschiedlichen Wasserstoffbrückenbindungsstärken der Tenside zu unterschiedlichen Penetrationstiefen in die Wasseroberfläche führen. Dies könnte die Wasserstruktur an der Oberfläche stören und zu größerer Unordnung führen, womit das SFG Signal abgeschwächt würde. Zusätzlich wurde das Verhältniss der spektralen Flächen der CH_2 symmetrischen Streckschwingung (d^+) und der CH_3 symmetrischen Streckschwingung (r^+) als ein Indikator für Ordnung innerhalb der Monolage genutzt. In einer Monolage, in welcher die Tenside in einer vollständigen trans-Konformation vorliegen, sind alle Methylengruppen in einer pseudo zentrosymmetrischen Umgebung und leisten somit keinen Beitrag zum SFG Spektrum. Die Methylgruppen wiederum sind geordnet und in einer nicht zentrosymmetrischen Umgebung und leisten somit maximalen Beitrag zum Spektrum. Ein hohes d^+ zu r^+ Verhältnis bedeutet somit, dass mehr Gauche-Defekte vorhanden sind und damit mehr Unordnung in der Monolage herrscht.

Schließlich wurde mit phasensensitiver SFG ein positives Band für alle Tensidmischungen im $\text{Im}\chi^{(2)}$ Spektrum gefunden, welches zwischen 2300 cm^{-1} und 2350 cm^{-1} zentriert ist. Da dieses Band für reines Wasser ein negatives Vorzeichen hat, wurde das positive Vorzeichen dem Einfluss der Tenside auf die Ausrichtung von Wasser zugerechnet. Es könnte darauf hindeuten, dass aufgrund von Wasserstoffbrückenbindungen zu den funktionellen Gruppen der Tenside Wassermoleküle ihre Orientierung ändern.

Acknowledgements

First of all I want to thank Prof. Dr. Mischa Bonn for giving me the opportunity to do my master thesis at the Max Planck Institute for Polymer Research and reviewing this thesis. Additionally I want to thank Prof. Dr. Thomas Basché for also reviewing this thesis.

I would like to express my gratitude to my supervisors Dr. Yuki Nagata and Dr. Johannes Hunger for always having an open door and granting me deeper insights into the topics at hand.

I want to specially thank Veronika Wank for investing a lot of time in helping me with phase-sensitive SFG measurements and having great patience. Furthermore I want to thank Takazu Seki, Xiaoqing Yu and Chun-Chieh Yu for always taking the time for answering my questions and teaching me on using SFG. Next I want to thank Prerna Sudera and Daria Maltseva for teaching me how to use the Tensiometer. Lastly I want to thank my friends and family for emotional support and allowing me to rely on them.

Contents

1	Introduction and Motivation	1
2	Theoretical Background	3
2.1	Surface Energy	3
2.1.1	Real Systems and Gibbs Model	3
2.2	Tensiometry	6
2.2.1	Phase transition of 1-Dodecanol at the air-water interface	7
2.3	Vibrational Sum Frequency Generation Spectroscopy	8
2.3.1	Resonant and Non-resonant Susceptibility	11
2.3.2	Surface Specificity	11
2.3.3	Polarization	12
2.3.4	Phase-resolved SFG	12
2.3.5	Fitting	14
2.4	Vibrational Modes	15
2.4.1	Methyl and Methylene Modes	15
2.4.2	The Water-Air Interface	16
3	Results and Discussion	19
3.1	Tensiometry	19
3.2	SFG Spectroscopy	21
3.2.1	CH Stretch Domain	21
3.2.2	Bonded OH Domain	25
3.2.3	OD and CH Stretch Domain	27
3.2.4	Phase-sensitive SFG	32
4	Conclusion and Outlook	37
5	Methods	39
5.1	Sample Preparation	39
5.1.1	H ₂ O dodecanol solution	39
5.1.2	H ₂ O dodecylamine solution	39
5.1.3	D ₂ O dodecanol solution	39
5.1.4	D ₂ O dodecylamine solution	39
5.2	Tensiometry	39
5.3	Direct SFG	40
5.3.1	Experimental Procedure	41
5.3.2	Data Processing	41
5.4	Phase-sensitive SFG	42
5.4.1	Data Processing	42
	Appendix	45

Abbreviations

SFG	sum frequency generation spectroscopy
VSFG	vibrational sum frequency generation spectroscopy
DPPG	1,2-dipalmitoyl- <i>sn</i> -glycero-3-phospho-(1'- <i>rac</i> -glycerol)
DPTAP	1,2-dipalmitoyl-3-trimethylammonium-propane chloride salt
C ₁₂ TAB	dodecyltrimethylammonium bromide
SDS	sodium dodecylsulfate
DOH	dodecanol
DA	dodecylamine
DAH	dodecylamine hydrochloride
HAD	hexadecylamine
LC phase	liquid condensed phase
LE phase	liquid expanded phase
G phase	gaseous phase
IR	infrared light
VIS	visible light
SHG	second harmonic generation
PS-SFG	phase-sensitive sum frequency generation spectroscopy
LO	local oscillator
Re	real
Im	imaginary
FR	Fermi resonance
DCM	dichloromethane
BAM	brewster angle microscopy
MD	molecular dynamics
IFFT	inverse fast Fourier transformation
FFT	fast Fourier transformation

Chapter 1

Introduction and Motivation

The water-air interface is the most common liquid interface on the earth and it critically impacts atmospheric, aerosol and environmental chemistry.[1] Furthermore, water is not only essential for life, but also the most common laboratory solvent. Single water molecules are quite well understood but in condensed matter water builds extended hydrogen bonded networks, which lead to unique properties, such as ice being less dense than liquid water, or the unusual high surface tension.[2] Understanding the water-air interface is of great importance to biology, chemistry, physics and other scientific fields because of the ubiquity of said interface.[3]

In this work, the effect of non ionic surfactant mixtures at the water-air interface on the ordering of water molecules and the ordering of the surfactant monolayer itself are examined using surface tension measurements as well as the powerful vibrational sum frequency generation spectroscopy. The word surfactant means **surface active agent** and describes molecules that reduce surface tension. Because of that, surface tension measurements are a natural first choice to analyse surfactant molecules at the water-air interface. Furthermore, vibrational sum frequency generation spectroscopy is a powerful tool for probing interfaces, because the inherent selection rules only allow sum frequency generation in a non centrosymmetric environment, i.e. the interface. Therefore no signal from the bulk is generated and the interface can be probed independently. Vibrational sum frequency generation spectroscopy yields a surface specific vibrational spectrum, which allows for unique possibilities to gather information on the interface.

The interaction between surface active compounds such as lipids and other surfactants is crucial for understanding biological lipid membrane-water interfaces, which are important in many biological processes. Additionally surfactants have a widespread commercial use as detergents, wetting agents, emulsifiers and foaming agents.

The effects of ionic surfactant mixtures on the water structure is fairly well investigated, but there is no understanding of the effects of electro neutral surfactant mixtures. The intent of this work is to investigate these effects using simple surfactants and gain a better understanding of the influences of biological membranes or commercial detergents on the water structure. Biological membranes mainly consist of neutral, zwitterionic and negatively charged lipids that self-assemble into a bilayer in contact with water. The effects of oppositely charged lipid mixtures on water alignment have been studied by Dreier and coworkers using direct SFG.[4] They found a diminishing SFG signal in the bonded OD region for lipid mixtures with a minimum for an one to one ratio of negatively charged DPPG [1,2-dipalmitoyl-*sn*-glycero-3-phospho-(1'-*rac*-glycerol) sodium salt] and positively charged DPTAP (1,2-dipalmitoyl-3-trimethylammonium-propane chloride salt). This is explained by the Coulomb force of the charged lipids aligning the molecular dipoles. At 1:1 mixture there is no net charge and therefore the water molecules are not aligned by the Coulomb interaction.[4]

Fausser and coworkers analysed the effects of mixtures of the oppositely charged surfactants dodecyltrimethylammonium bromide(C₁₂TAB) and sodium dodecylsulfate (SDS), on surface tension. They found a significant lower surface tension for mixtures than for the neat surfactant solutions, and a general higher surface activity even for concentrations where neat surfactants

show no surface activity. This behaviour was explained by synergistic adsorption of head-head catanionic complexes.[5]

For the ionic surfactants the long range Coulomb interaction is always the dominant effect on water alignment. In the present study the simple model non-ionic surfactants dodecanol and dodecylamine are used to analyse the effects of monolayers of uncharged surfactant mixtures.

Chapter 2

Theoretical Background

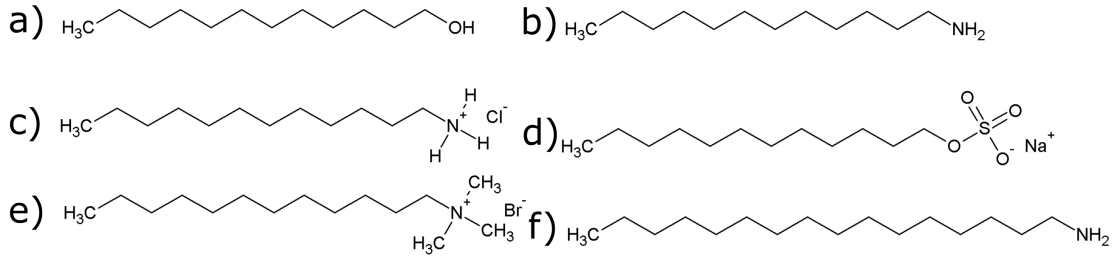


Figure 2.1: Surfactant molecules mentioned in this work. a) Dodecanol (DOH) b) Dodecylamine (DA) c) Dodecylamine hydrochloride (DAH) d) Sodium dodecyl sulfate (SDS) e) Dodecyltrimethylammonium bromide (C₁₂TAB) f) Hexadecylamine (HAD).

2.1 Surface Energy

The attractive forces acting between molecules are orders of magnitude larger in the liquid and solid phase than in the gaseous phase. In the bulk phase a molecule is on average surrounded by molecules, so that the potential energy minimum is reached. At the gas-condensed phase-interface, a surface molecule of the condensed phase is in contact with less molecules, because of the lower density of molecules in the gaseous phase. This leads to a higher potential energy due to less attractive forces (see figure 2.1).[6]

Consider a liquid film, being stretched in a wire frame (see figure 2.3). Applying a force F to the wire frame and displacing it by dx requires the energy Fdx . This is opposed by the increase in surface area dA times the surface energy ϵ .

$$Fdx = \epsilon dA \quad (2.1)$$

Rearranging equation 2.1 gives an expression for the surface energy.

$$\epsilon = F \frac{dx}{dA} \quad (2.2)$$

Surface energy ϵ and surface tension γ are equal, when a state of equilibrium is reached.[6]

2.1.1 Real Systems and Gibbs Model

Consider a mixture of water and a generic simple alcohol. The liquid bulk phase contains n_1 moles of water and n_2 moles of alcohol and is macroscopically homogeneous when in equilibrium. Above

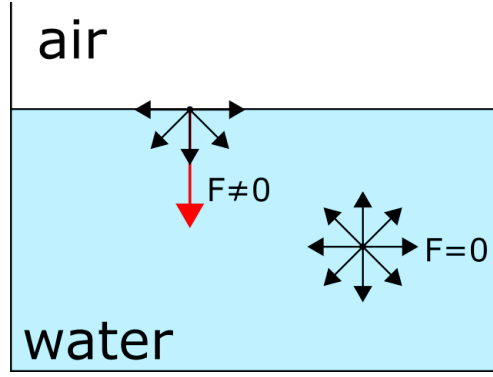


Figure 2.2: Schematic drawing of the attractive forces which result in a net inward force and thus a higher potential energy for surface molecules.[6]

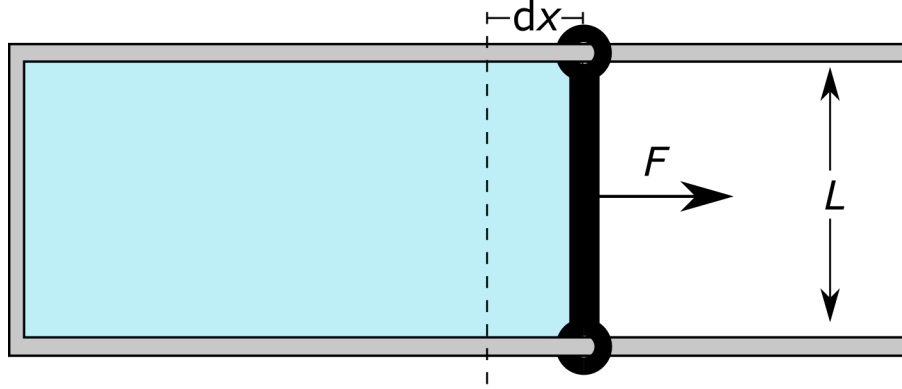


Figure 2.3: Schematic drawing of a liquid film stretched in a wireframe.[6]

the liquid a vapour phase will form, which will contain n'_1 moles of water and n'_2 of alcohol. Since the generic alcohol is more volatile than water, it is expected that the mole fraction of alcohol is higher in the vapour phase than in the liquid phase.

For less volatile components the partial vapour pressure will be so small that the concentration in the vapour phase c' is negligible compared to the concentration in the liquid phase c .

$$\frac{n'_2}{n'_1} > \frac{n_2}{n_1} \quad (2.3)$$

Then the surface phase can be imagined as J numbers of homogeneous layers, where each layer contains Δn_1^J moles of water and Δn_2^J moles of alcohol. The total molarity in the surface layer is given by equation 2.4 and 2.5.

$$\Delta n_1 = \Delta n_1^1 + \Delta n_1^2 + \dots + \Delta n_1^J \quad (2.4)$$

$$\Delta n_2 = \Delta n_2^1 + \Delta n_2^2 + \dots + \Delta n_2^J \quad (2.5)$$

Due to the inhomogeneity of the interface, the sublayers are not equal.

$$\frac{\Delta n_2^1}{\Delta n_1^1} \neq \frac{\Delta n_2^2}{\Delta n_1^2} \neq \dots \neq \frac{\Delta n_2^J}{\Delta n_1^J} \quad (2.6)$$

Therefore, the bulk phase and the surface phase can be distinguished based on whether they are homogeneous or inhomogeneous.

A real interface between two bulk phases A and B is not one surface but rather each bulk phase has their respective surfaces AA' and BB', so the interface can be described as AA'BB' (see figure 2.4 a)). One possible simplified model is the Gibbs model, where the surface phase is considered of having zero thickness. In this model the interface can be described as GG', where GG' is a mathematical plane, which is placed parallel to AA' or BB' and is called the Gibbs dividing surface. Figure 2.4 shows a side by side comparison between a) the real system and b) the idealised Gibbs model b). The curve in the real system represents the change of any extensive property which has to change continuously and cannot have an abrupt change. In the simplified Gibbs model there is an abrupt change at the Gibbs dividing surface. Extensive properties depend linearly on the size of the system.[7]

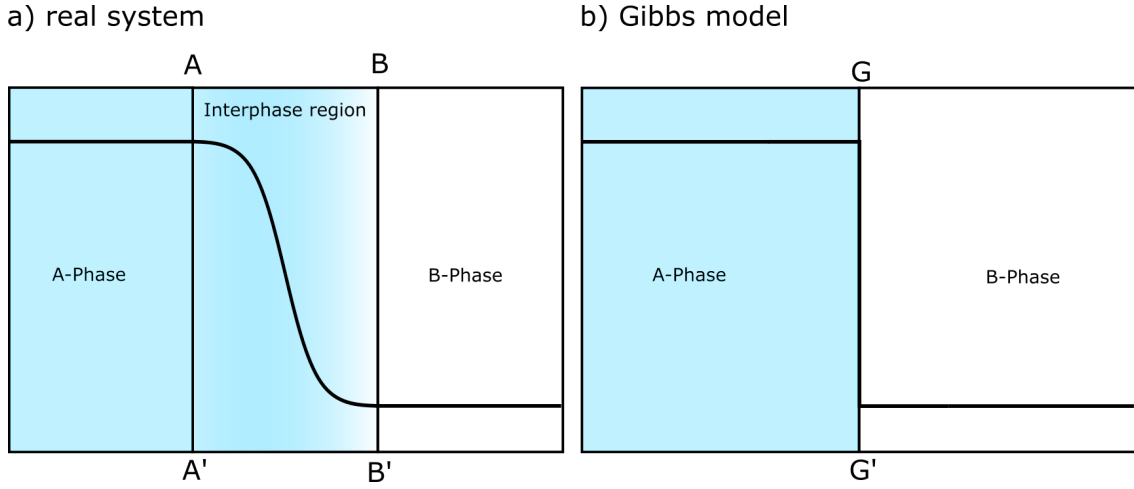


Figure 2.4: a) Real system with the inhomogeneous surface phase AA'BB'. b) Idealized Gibbs model of the liquid column with the Gibbs dividing surface GG'. [6] [7]

In this model the composition of the phases remains unchanged until GG' is reached. If the interface of a liquid binary mixture is regarded as an additional phase, the Gibbs-Duhem-equation (eq. 2.7) can be used to connect chemical potential μ and surface tension γ .

$$-Ad\gamma = N_1^s d\mu_1 + N_2^s d\mu_2 \quad , \text{constant } T, p \quad (2.7)$$

where γ is the surface tension, A is the surface area, N_1^s and N_2^s are the number of moles of solvent and solute at the surface. When the surface phase is in equilibrium with the liquid bulk phase, the chemical potential can also be related with the Gibbs-Duhem-equation of the bulk phase (eq. 2.8).

$$0 = N_1 d\mu_1 + N_2 d\mu_2 \quad \text{constant } T, p \quad (2.8)$$

with N_1 and N_2 being the number of moles in the bulk. Rearranging equation 2.8 yields equation 2.9.

$$d\mu_1 = -d\mu_2 \frac{N_2}{N_1} \quad (2.9)$$

Inserting equation 2.9 in equation 2.7 leads to the Gibbs adsorption equation.

$$-d\gamma = \left(\frac{N_2^s}{A} - \frac{N_1^s}{A} \frac{N_2}{N_1} \right) d\mu_2 \quad (2.10)$$

The Gibbs surface excess of the surfactant $\Gamma_2^{(1)}$ is defined by equation 2.11.

$$\Gamma_2^{(1)} = \Gamma_2 - \Gamma_1 \cdot \frac{N_2}{N_1} \quad (2.11)$$

And the absolute two dimensional surface concentrations Γ_i can be described as follows:

$$\Gamma_i = \frac{N_i^s}{A} \quad (2.12)$$

With the expressions in equation 2.11 and equation 2.12, the Gibbs adsorption equation (eq. 2.10) can be simplified to:

$$\Gamma_2^{(1)} d\mu_2 = -d\gamma \quad (2.13)$$

To obtain Gibbs surface excess Γ_2^1 (equation 2.15), equation 2.14 is substituted in Gibbs adsorption equation 2.13.

$$\mu_2 = \mu_2^0 + RT \ln a_2 \quad (2.14)$$

$$\Gamma_2^{(1)} = -\frac{1}{RT} \frac{d\pi}{d \ln a_2} \quad (2.15)$$

a_2 is the activity of the surfactant, and is the product of the molar fraction in the bulk x_2 and the activity coefficient $\gamma_2(x_2)$. In equation 2.15 the surface tension γ is replaced with the surface pressure π . Therefore, the surface excess is dependent on the slope of the Gibbs adsorption isotherm, which is the surface pressure plotted against bulk concentration or activity. [8]

2.2 Tensiometry

To measure the surface pressure or tension, there are multiple possible geometries for measurements, for example Wilhelmy slide method [9], contact angle measurement[10], or pendent drop method[11]. In this work a variation on the Wilhelmy slide method suggested by Padday and coworkers is used.[12] Here, a thin oxide coated metal rod is suspended from a micro balance and is brought into contact with the liquid surface. Figure 2.5 shows a schematic drawing of the forces acting on the rod, where F_p is the resulting force on the probe, F_b is the force resulting from buoyancy, m_m is the weight of the meniscus under the rod, r is the radius of the rod and ϕ is the angle between the meniscus and the horizontal of the rod.[12]

For the measurement of the surface tension it is important to measure at the same height above the surface, so that the influence of the buoyancy F_b and the weight of the meniscus m_m are consistent. The weight of the meniscus m_m can be described as;

$$m_m = \pi r^2 z \rho \quad (2.16)$$

where ρ is the density difference between the liquid and the surrounding fluid.[12] Assuming the ideal case where no wetting of the sides of the rod occur (Figure 2.5 on the right), the force on the probe is given by the weight of the rod, which does not change significantly, the weight of the meniscus and the effect of surface tension, and can be described as;

$$F = m_m g + 2\pi r \gamma \sin \phi \quad (2.17)$$

where g is the local gravity, and γ is the surface tension of the liquid. In this work the surface pressure π is measured rather than the surface tension γ . The surface pressure exerted by a film at the liquid-gas interface π can be described as;

$$\pi = \gamma_0 - \gamma \quad (2.18)$$

where γ_0 is the surface tension of the solvent without a film and γ is the surface tension with a film present.[6]

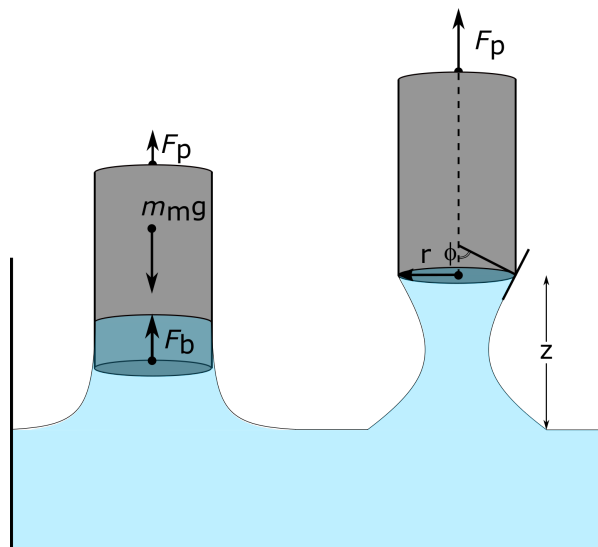


Figure 2.5: Schematic drawing of geometry of the used tensiometer, as described by Padday and coworkers.[12]

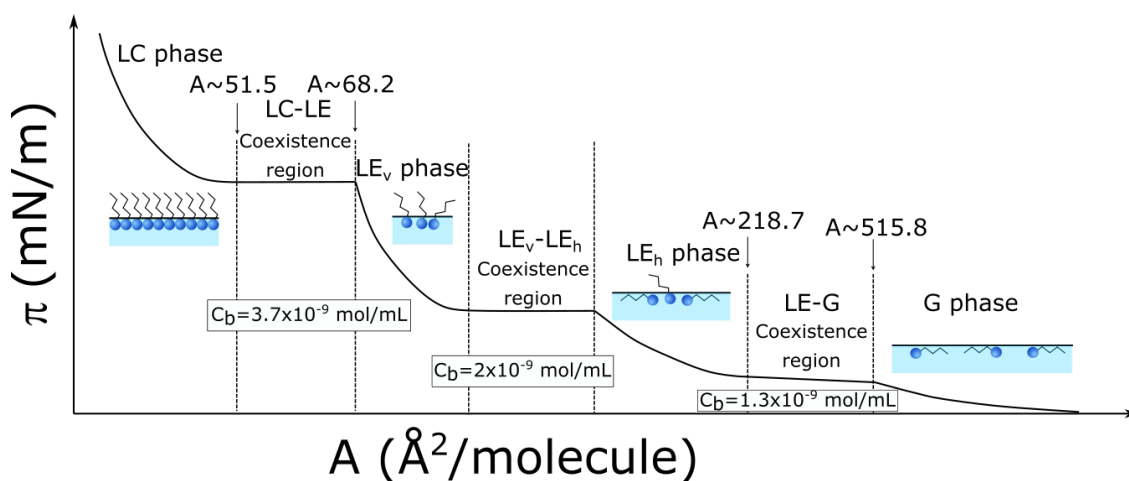


Figure 2.6: The phase transition mechanism of a 1-dodecanol monolayer at the air water interface at 20 °C taken from Wu and coworkers.[13]

2.2.1 Phase transition of 1-Dodecanol at the air-water interface

The surface pressure π of an adsorbed monolayer is directly related to the area per molecule A and therefore the packing density of the monolayer. The monolayer changes its phase upon a certain increase in packing density. Figure 2.6 shows a schematic graph of surface pressure of aqueous dodecanol solutions plotted against the area per molecule, taken from Wu and coworkers[13]. With increasing bulk concentration the area per molecule decreases and the surface pressure rises. There are regions of coexistence between two different phases which show a plateau of constant surface pressure. Regions that have a single phase show an increase of surface pressure with decreasing area per molecule. With relatively low surface coverage of up to $515.8 \text{ \AA}^2/\text{molecule}$ the surfactant molecules are in a gaseous (G) phase, where the molecules lie flat on the surface and do not interact with one another. Up to $218.7 \text{ \AA}^2/\text{molecule}$ gaseous (G) and horizontal liquid expanded phase (LE_h) coexist. For 1-dodecanol this phase transition happens for a bulk concentration of

1.3×10^{-9} mol/mL and corresponds to a surface pressure of 0.75 mN/m. The phase transition between horizontal liquid expanded phase (LE_h) and vertical liquid expanded phase (LE_v) happens at a bulk concentration of 2×10^{-9} mol/mL. The LE_v phase to liquid condensed phase (LC) transition happens between $68.2 \text{ \AA}^2/\text{molecule}$ and $51.5 \text{ \AA}^2/\text{molecule}$ and a bulk concentration of 3.7×10^{-9} mol/mL. This phase transition corresponds to a surface pressure of 17.9 mN/m. [13][14]

The driving force for the surfactants to stand upright at higher surface coverages is the concentration and the Van der Waals forces between tightly packed hydrocarbon tails stabilize the upright position.[13]

2.3 Vibrational Sum Frequency Generation Spectroscopy

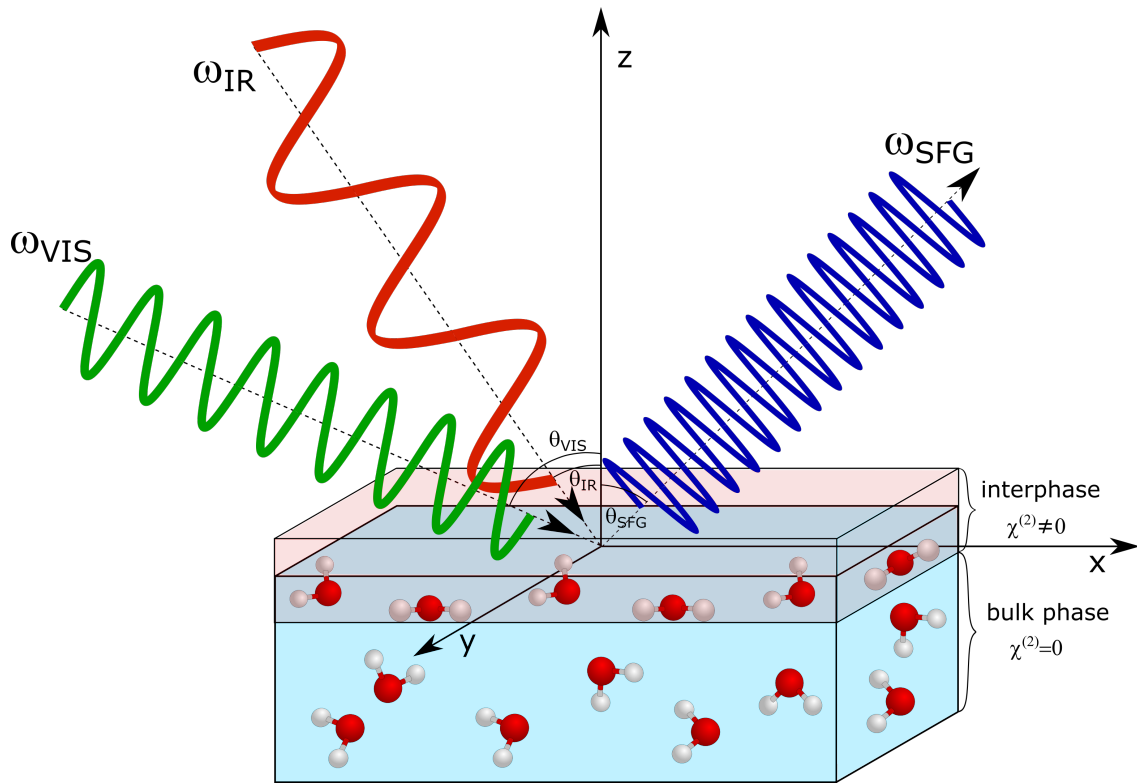


Figure 2.7: Schematic drawing of the underlying principle of vibrational sum frequency generation spectroscopy.[15]

Vibrational sum frequency generation spectroscopy (VSFG) is a non linear process where two beams of different energies generate an output beam.

The technique uses fundamental differences in symmetry for bulk-phases and interfaces to generate a vibrational spectrum of the interface only. Because of the surface specificity, sum frequency generation spectroscopy is a powerful tool for probing interfaces, and is used in a wide variety of fields including chemistry, biology, physics and electronics.[16] The method is extremely sensitive to surfactant molecules at the surface and can be used to detect less than a monolayer of molecules adsorbed to the surface. [17]

Nonlinear optics goes back to Franken and coworkers, who first described second harmonic generation (SHG) in a quartz crystal.[18] Second harmonic generation is closely related to sum frequency generation, and uses two photons of the same energy to generate a photon with twice the energy.[19] However, second harmonic generation was not used as a surface probe until 1981 and sum frequency generation until 1987.[16]

In the years since, the technique was improved further and the necessary theory was developed. This development continues to the present day and SFG is widely used and is still being improved.[16]

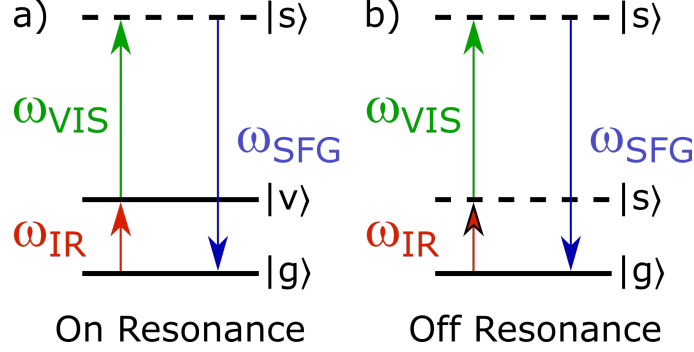


Figure 2.8: Energy level diagram of the sum frequency generation process a) on and b) off resonance.[15]

Sum frequency generation is achieved by overlapping two pulsed laser beams spatially and temporally at an interface. The two beams used are a visible laser with a fixed frequency ω_{VIS} and a tunable infrared laser with the frequency ω_{IR} . The frequency of the generated SFG light is the sum of both the IR and VIS light (equation 2.19).[15]

$$\omega_{\text{SFG}} = \omega_{\text{VIS}} + \omega_{\text{IR}} \quad (2.19)$$

Figure 2.8 shows an energy level diagram for the SFG process a) on resonance and b) off resonance. When the IR frequency coincides with a vibrational transition between the vibrational ground state $|g\rangle$ and the vibrational excited state $|v\rangle$ of a molecule at the interface, the intensity is resonantly enhanced. $|s\rangle$ represents virtual states, which are no eigenfunctions of the Hamiltonian, and are therefore very short lived and cannot be directly observed. Detecting the sum frequency light as a function of the tunable IR frequency yields a vibrational spectrum that is up-converted into the visible range.[15]

Because SFG is a non linear vibrational spectroscopy, different selection rules apply than for linear vibrational spectroscopies, such as infrared and Raman spectroscopy. The central selection rule for SFG is that a vibrational mode needs to be non centrosymmetric or in an asymmetric environment to be SFG active and for resonance to occur. This needs to be the case for both macroscopic and microscopic scales.[15]

Classic liquid bulk phases have an isotropic distribution of molecules and thus are centrosymmetric, and, therefore, do not fulfil the SFG selection rule. Introducing an interface breaks the inherent symmetry of the bulk phase and vibrational modes may become SF active. On a microscopic level there needs to be a net orientation of the surface molecules. A random orientation of molecules at a surface would not yield a SFG signal, because the signals of molecules with different orientation cancel each other out and there is no net orientation. A certain degree of ordering is required for a SF signal to be generated, however complete ordering of oppositely oriented molecules would lead to the signals cancelling each other out.[15]

The topmost layer of water experiences some degree of ordering to compensate for missing water molecules in the hydration shell of the surface molecules. Therefore, a SFG spectrum of neat water can be obtained. The water SFG spectrum is discussed more thoroughly in section 2.4.2.

SFG is a coherent process and its signal has a direction, phase and magnitude related to that of the incident beams. The electric field \vec{E} of light propagating through a medium exerts a force on the valence electrons and the nuclei of a molecule which causes an induced dipole μ . For the deformation of the electron shell induced by an electric field, the movement of the nuclei can be neglected because of the Born-Oppenheimer approximation, which states that the nucleus is

orders of magnitude heavier than the electrons and therefore moves much slower and is assumed as static.[15]

In this thesis the electric dipole approximation is used to describe the interaction between matter and electromagnetic waves. Hence, the effects of optical magnetic fields and electric multipoles (e.g. quadrupoles) are not taken into account. Also contributions of electric fields of neighbouring molecules are ignored and it is assumed that only the macroscopic field induces the molecular dipole.[15] In an isotropic medium this dipole is given by:

$$\mu = \mu_0 + \alpha E \quad (2.20)$$

with the permanent dipole μ_0 and the polarizability of the molecular electrons α . In condensed phase the sum of molecular dipoles causes a macroscopic polarization of the medium \vec{P} , given by equation 2.21.[15]

$$\vec{P} = \epsilon_0 \chi^{(1)} \vec{E} \quad (2.21)$$

where ϵ_0 is the vacuum permittivity and $\chi^{(1)}$ is the macroscopic average of the molecular polarizabilities α . $\chi^{(1)}$ is also known as the first-order or linear susceptibility. The induced dipole in a molecule oscillates at the frequency of the electric field and the molecule acts like a hertz dipole so that it can emit light at said frequency. For weak electric fields non-linear effects are negligible and equation 2.21 fully describes the polarizability. For an increasing field strength higher order effects must be included for the induced dipole μ (eq. 2.22) and the macromolecular polarizability \vec{P} (eq. 2.23). These strong electric fields are usually achieved with pulsed lasers.

$$\mu = \mu_0 + \alpha \vec{E} + \beta \vec{E}^2 + \gamma \vec{E}^3 + \dots \quad (2.22)$$

$$\begin{aligned} \vec{P} &= \epsilon_0 (\chi^{(1)} \vec{E} + \chi^{(2)} \vec{E}^2 + \chi^{(3)} \vec{E}^3 + \dots) \\ &= \vec{P}^{(1)} + \vec{P}^{(2)} + \vec{P}^{(3)} + \dots \end{aligned} \quad (2.23)$$

where β and γ are the second- and third-order hyperpolarizabilities and $\chi^{(2)}$ and $\chi^{(3)}$ are the second- and third-order non-linear susceptibilities.

The surface electric field \vec{E}_{SFG} can be described as the sum of the two incident electric fields \vec{E}_{VIS} and \vec{E}_{IR} with the frequencies ω_{VIS} and ω_{IR} in equation 2.24.

$$\vec{E}_{\text{SFG}} = \vec{E}_{\text{VIS}} \cos \omega_{\text{VIS}} t + \vec{E}_{\text{IR}} \cos \omega_{\text{IR}} t \quad (2.24)$$

Since SFG is based on the interaction with two fields, it is determined by the second order polarizability $\vec{P}_{\text{SFG}}^{(2)}$. Considering only the second order polarizability $\vec{P}_{\text{SFG}}^{(2)}$ and substituting equation 2.24 gives following expression.[20]

$$\vec{P}_{\text{SFG}}^{(2)} = \epsilon_0 \chi^{(2)} (\vec{E}_{\text{VIS}} \cos \omega_{\text{VIS}} t + \vec{E}_{\text{IR}} \cos \omega_{\text{IR}} t)^2 \quad (2.25)$$

By not specifically including the time dependence of the second-order polarization $\vec{P}_{\text{SFG}}^{(2)}$ equation 2.25 can be simplified to equation 2.26.

$$\vec{P}_{\text{SFG}}^{(2)} = \epsilon_0 \chi^{(2)} \vec{E}_{\text{VIS}} \vec{E}_{\text{IR}} \quad (2.26)$$

If the IR and VIS beam spatially and temporally overlap, sum frequency signal is generated at an angle θ_{SFG} to the surface normal. Using conservation of momentum this angle can be calculated with the phase-matching condition displayed in equation 2.27.[15]

$$n_{\text{SFG}} \omega_{\text{SFG}} \sin \theta_{\text{SFG}} = n_{\text{VIS}} \omega_{\text{VIS}} \sin \theta_{\text{VIS}} \pm n_{\text{IR}} \omega_{\text{IR}} \sin \theta_{\text{IR}} \quad (2.27)$$

where n is the refractive index of the medium the beam propagates through, ω is the frequency and θ is the angle to the surface normal, displayed in figure 2.7. Equation 2.26 fully describes the sum frequency generation from a surface, but does so independent of a surface bound coordinate

system. Since the incident beams are angled with regard to the surface normal, it is useful to introduce a surface bound cartesian coordinate system.

$$\vec{P}_{\text{SFG}}^{(2)} = \sum_i^{x,y,z} \vec{P}_{i,\text{SFG}}^{(2)} = \epsilon_0 \sum_i^{x,y,z} \sum_j^{x,y,z} \sum_k^{x,y,z} \chi_{ijk}^{(2)} \vec{E}_{j,\text{VIS}} \vec{E}_{k,\text{IR}} \quad (2.28)$$

Equation 2.28 contains all 27 possible combinations of x , y and z for i , j and k . To simplify only one representative combination is used. However, all combinations are needed to calculate the SFG signal (eq. 2.29).

$$\vec{P}_{i,\text{SFG}}^{(2)} = \epsilon_0 \chi_{ijk}^{(2)} \vec{E}_{j,\text{VIS}} \vec{E}_{k,\text{IR}} \quad (2.29)$$

2.3.1 Resonant and Non-resonant Susceptibility

The presented derivations are true for molecules adsorbed at a SF inactive interface. However, many surfaces show a inherent SF activity. To include this SF activity an additional susceptibility is introduced. This susceptibility is of non-resonant nature and is termed $\chi_{\text{NR}}^{(2)}$. The total susceptibility $\chi^{(2)}$ is the sum of the resonant $\chi_{\text{R}}^{(2)}$ and the non-resonant susceptibility $\chi_{\text{NR}}^{(2)}$. [15]

$$\chi^{(2)} = \chi_{\text{R}}^{(2)} + \chi_{\text{NR}}^{(2)} \quad (2.30)$$

The resonant susceptibility $\chi_{\text{R}}^{(2)}$ is proportional to the frequency dependent part shown in equation 2.31.

$$\chi_{\text{R}}^{(2)} \propto \frac{1}{(\omega_{\text{v}} - \omega_{\text{IR}} - i\Gamma)} \quad (2.31)$$

where ω_{v} is the frequency of the vibrational mode, ω_{IR} is the variant IR frequency and Γ is the damping constant. When ω_{IR} equals ω_{v} the $\omega_{\text{IR}} - \omega_{\text{v}}$ becomes zero and the magnitude of $\chi_{\text{R}}^{(2)}$ greatly increases.

The resonant and non-resonant susceptibility can be expressed in polar coordinates for easier visualization in the complex plane: [15]

$$\chi_{\text{R}}^{(2)} = |\chi_{\text{R}}^{(2)}| e^{i\delta} \quad (2.32)$$

$$\chi_{\text{NR}}^{(2)} = |\chi_{\text{NR}}^{(2)}| e^{i\epsilon} \quad (2.33)$$

The intensity of the SF signal is proportional to the the absolute square of the sum of both the resonant $\chi_{\text{R}}^{(2)}$ and non-resonant $\chi_{\text{NR}}^{(2)}$ susceptibility.

$$I_{\text{SF}} = |\vec{E}_{\text{SF}}|^2 \propto |\chi^{(2)}|^2 = ||\chi_{\text{R}}^{(2)}| e^{i\delta} + |\chi_{\text{NR}}^{(2)}| e^{i\epsilon}|^2 \quad (2.34)$$

For the direct SFG spectrum the sample signal is normalized by dividing by a quartz reference. [20]

$$I_{\text{direct}} = \frac{|\chi_{\text{sample}}^{(2)}|}{|\chi_{\text{quartz}}^{(2)}|} \quad (2.35)$$

2.3.2 Surface Specificity

Even though the non-linear susceptibility contains 27 components, due to symmetry considerations the number of non zero contributions is lower. In a centrosymmetric medium all directions are equivalent, and therefore two opposing directions must be equal.

$$\chi_{ijk}^{(2)} = \chi_{-i-j-k}^{(2)} \quad (2.36)$$

Changing the sign of all three subscripts is equivalent to reversing the axis system and therefore the physical phenomenon $\chi_{ijk}^{(2)}$ describes, reverses its sign.[15]

$$\chi_{ijk}^{(2)} = -\chi_{-i-j-k}^{(2)} \quad (2.37)$$

To generate a SF signal both equation 2.36 and 2.37 must be fulfilled. In a centrosymmetric medium this is only true if $\chi_{ijk}^{(2)} = 0$, and therefore a centrosymmetric medium is SF inactive. An isotropic surface has S_∞ symmetry, which means that $x = -x$, $y = -y$ and $z \neq -z$. With the asymmetry in z-direction there are four independent non zero contributions of $\chi_{ijk}^{(2)}$: [15]

$$\chi_{zxx}^{(2)} (= \chi_{zyy}^{(2)}), \quad \chi_{xzx}^{(2)} (= \chi_{yzy}^{(2)}), \quad \chi_{xxz}^{(2)} (= \chi_{yyz}^{(2)}), \quad \chi_{zzz}^{(2)}$$

2.3.3 Polarization

Utilizing polarized light, different components of the $\chi_{ijk}^{(2)}$ can be resolved. Figure 2.9 shows two possible polarizations used in SFG, a) s-polarized light with the electric field vector of the incident wave \vec{E}_I perpendicular to the plane of incidence and b) p-polarized light with the electric field vector of the incident wave \vec{E}_I parallel to the plane of incidence.

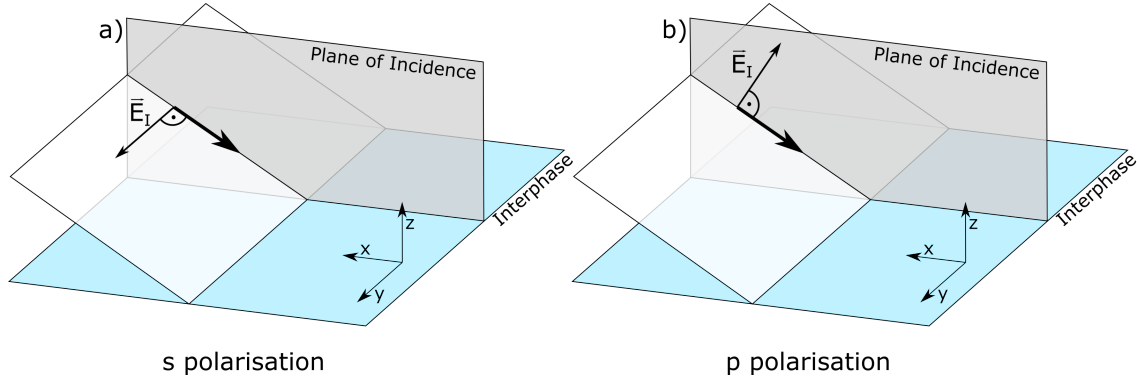


Figure 2.9: Schematic drawing of a) a perpendicular s-polarized incident electric field \vec{E}_I and b) a parallel p-polarised incident electric field \vec{E}_I .

S-polarized light only has a y-component and p-polarized light has both a x- and a z-component. In this thesis only the ssp-polarization is used.

Table 2.1: All possible polarization combinations and their elements of $\chi_{ijk}^{(2)}$ that contribute to the spectrum. The polarization combinations are in order SFG, VIS and IR.[15]

Polarization combination	Elements of $\chi_{ijk}^{(2)}$
pss	$\chi_{zyy}^{(2)}$
sps	$\chi_{yzy}^{(2)}$
ssp	$\chi_{yyz}^{(2)}$
ppp	$\chi_{zzz}^{(2)}, \chi_{zxx}^{(2)}, \chi_{xzx}^{(2)}, \chi_{xxz}^{(2)}$

2.3.4 Phase-resolved SFG

As shown in equation 2.34 in direct SFG spectroscopy the measured SFG intensity is proportional to the absolute square of the second order susceptibility $|\chi^{(2)}|^2$, this means that all information on the complex nature of $\chi^{(2)}$ is lost. This complex information can be retrieved by implementing

phase-sensitive sum frequency generation spectroscopy (PS-SFG) which was first introduced by Shen and coworkers.[21]

The phase-sensitivity is achieved by mixing the sample signal with a local oscillator (LO) of a known phase. The SFG signal I_{SF} equals the absolute square of the sample electric field \vec{E}_{sample} and the local oscillator electric field \vec{E}_{LO} . [22]

$$\begin{aligned} I_{\text{SF}} &= |\vec{E}_{\text{tot}}(\omega)|^2 = |\vec{E}_{\text{sample}} + \vec{E}_{\text{LO}}|^2 \\ &= |\vec{E}_{\text{sample}}|^2 + |\vec{E}_{\text{LO}}|^2 + \vec{E}_{\text{sample}}\vec{E}_{\text{LO}}^* \exp(i\omega T) + \vec{E}_{\text{sample}}^* \vec{E}_{\text{LO}} \exp(i\omega T) \end{aligned} \quad (2.38)$$

where $\vec{E}_{\text{sample}}^*$ and \vec{E}_{LO}^* are the complex conjugate of \vec{E}_{sample} and \vec{E}_{LO} . The exponential term $\exp(i\omega T)$ corresponds to the fringes seen in figure 2.10 and is introduced through a time delay of the sample SFG signal, before interfering with the local oscillator, achieved by using a silica plate. This time delay is crucial for the sample and local oscillator SFG signals to be separated. For ssp polarization combination $\chi^{(2)}$ is given by the following equation:[22]

$$\chi^{(2)} = \frac{F_{\text{sample}} r_{1,\text{sample}} r_{2,\text{sample}} \chi_{\text{yyz},\text{sample}}^{(2)}}{F_{\text{quartz}} r_{1,\text{quartz}} r_{2,\text{quartz}} \chi_{\text{yyz},\text{quartz}}^{(2)}} \quad (2.39)$$

where F is the product of Fresnel factors, $r_{j,X}$ is the complex reflectivity for the ω_j electric field and the surface X .

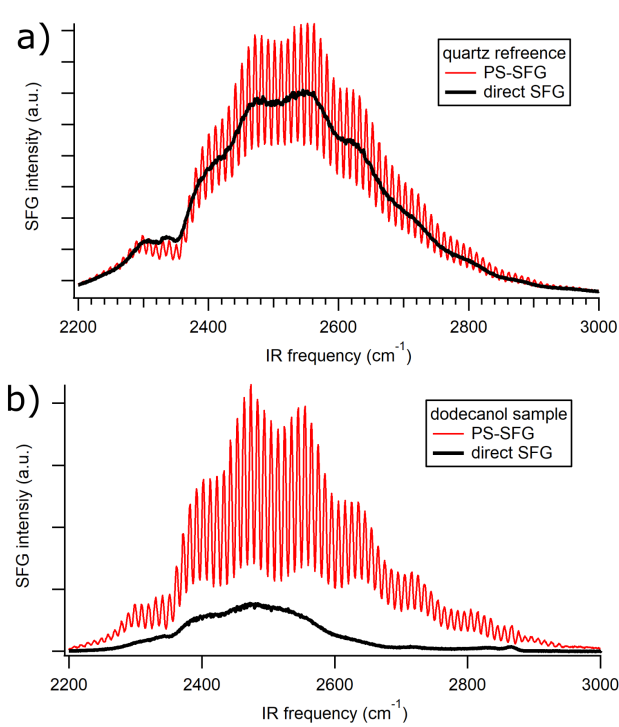


Figure 2.10: Non normalized direct and phase-sensitive SFG spectra of a) a quartz reference and b) a dodecanol monolayer on water. Both cases show deep fringes because the SFG response is comparable in magnitude to the local oscillator.

The imaginary part of the second order susceptibility $\text{Im}\chi^{(2)}$ contains information on vibrational resonances, and can therefore be directly compared to linear IR absorption measurements. Due to the real part of second order susceptibility $\text{Re}\chi^{(2)}$, peaks in the $|\chi^{(2)}|^2$ spectrum may be shifted and can therefore not be compared directly to linear vibrational spectroscopy.

From the sign of a peak in the $\text{Im}\chi^{(2)}$ the total orientation can be derived. For both direct and phase-resolved SFG a z-cut quartz crystal is used as a non-resonant reference to gain information of the spectral shape of the IR laser. In the phase-resolved case a phase correction of the complex phase between 90° and 115° is required because of the mismatch between the bulk-like response of the quartz and the surface-like response of the water-air interface.[20] In case of interfacial water, the free-OH peak can be used to check whether the phase correction was right, because the total orientation of this vibrational mode is well known.

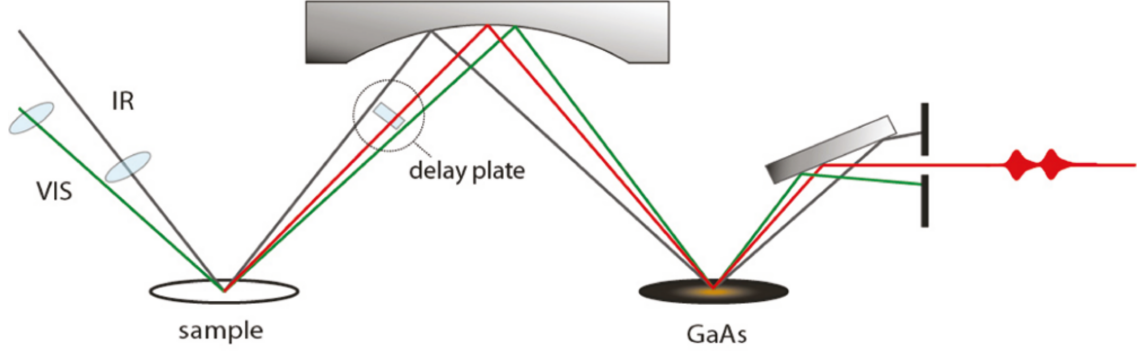


Figure 2.11: Geometry of the PS-SFG detection by Pool and coworkers.[20]

Figure 2.11 shows a PS-SFG geometry by Pool et al., where an infra-red and visible laser are overlapped in time and space at a sample surface and generate a SFG signal. The SFG signal is delayed by a silica plate and together with the reflected IR and VIS beam they are refocused by a spherical mirror on a medium with a frequency independent (non-resonant) second order non-linear response, such as gallium arsenide (GaAs). Here a second SFG (local oscillator) signal is generated that interferes with the sample SFG signal.[20]

2.3.5 Fitting

SFG spectra may be fitted with a Lorentzian model. Each vibrational mode (see equation 2.31) can be described as:[23]

$$\chi_i^{(2)}(\omega) = \frac{A_i}{\omega - \omega_i - \Gamma_i} \quad (2.40)$$

where A_i is the spectral area of the peak, ω_i is the frequency of the vibrational mode and Γ_i is the half width at half maximum.[23] The non-resonant part can be described as follows:

$$\chi_{\text{NR}}^{(2)} = A_{\text{NR}} e^{i\phi_{\text{NR}}} \quad (2.41)$$

The total direct SFG spectrum can than be described by the absolute square of the sum of the non resonant part and the vibrational modes.

$$|\chi^{(2)}(\omega)|^2 = |\chi_{\text{NR}}^{(2)}(\omega) + \chi_1^{(2)}(\omega) + \chi_2^{(2)}(\omega) + \dots|^2 \quad (2.42)$$

2.4 Vibrational Modes

2.4.1 Methyl and Methylene Modes

Figure 2.12 shows the CH stretch modes contributing to the dodecanol and dodecylamine SFG spectra. Different intensities for these peaks can give a clue on how the molecules are oriented and ordered at the surface.[24] In a LC phase monolayer the methylene stretch modes are in a pseudo centrosymmetric environment and are therefore weakened. Also in a LC phase monolayer the methyl groups are highly oriented and therefore show a intense peak in the monolayer. This means that the d^+/r^+ ratio can be used as a tool to probe changes in ordering for surfactant mixtures.[15]

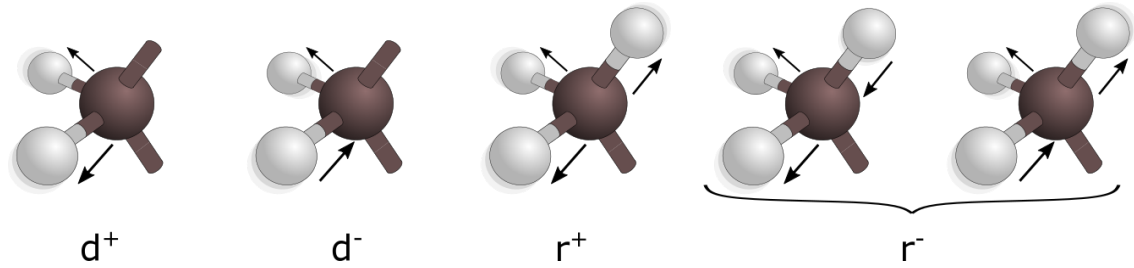


Figure 2.12: Methyl and Methylene stretch modes.[15][25]

Table 2.2: Methyl and Methylene stretch modes and their respective wavenumbers of an aliphatic chain in air.[15][25]

Mode	Description	Wavenumber (cm^{-1})
d^+	symmetric CH_2 stretch	2854
d_{FR}^+	symmetric CH_2 stretch (Fermi resonance)	2890-2930
d^-	anti symmetric CH_2 stretch	2915
r^+	symmetric CH_3 stretch	2878
r_{FR}^+	symmetric CH_3 stretch (Fermi resonance)	2942
r^-	anti symmetric CH_3 stretch	2966

In addition to the normal modes table 2.2 mentions Fermi resonance modes that are present in the CH stretch spectrum. Fermi resonance is an effect where a vibrational mode is split up by quantum mechanical mixing of the wave function of a vibrational mode with an overtone ($\Delta v = 2$ transition).

Figure 2.13 shows the mixing of the methyl symmetric stretch mode and the methyl bending overtone, which have similar energies. The degenerate modes split up into a low energy band at 2878 cm^{-1} , which is denoted as the symmetric stretch mode d^+ and a high energy band at 2942 cm^{-1} , denoted as the Fermi resonance band d_{FR}^+ . [25]

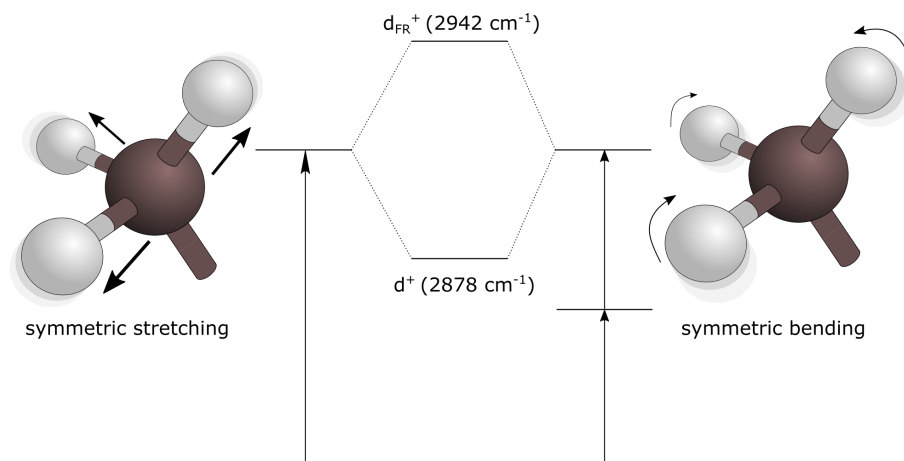


Figure 2.13: Schematic energy diagram of Fermi resonance of the methyl symmetric stretch.[25]

2.4.2 The Water-Air Interface

A single water molecule in the gas-phase possesses three vibrational modes shown in figure 2.14. A symmetric stretching vibration ν_1 at 3657.05 cm^{-1} , an anti-symmetric stretching mode ν_2 at 3755.97 cm^{-1} and a bending mode near 1595 cm^{-1} . [26]

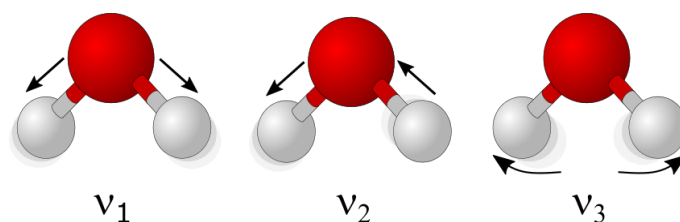
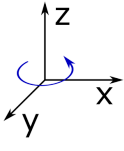
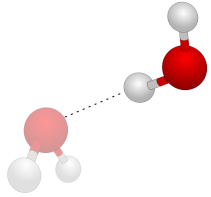
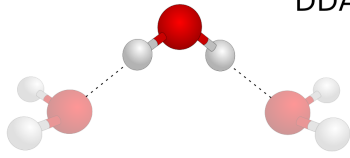


Figure 2.14: Vibrational modes of water.

Due to hydrogen bonding, these vibrations are red-shifted in bulk water and at the water interface. The spectrum of the water-air interface, shown in figure 2.15 (in this case D_2O -air interface), shows at least three different peaks. The sharp peak around 3700 cm^{-1} (2750 cm^{-1} in D_2O) can be attributed to the free-OH mode of a water molecule pointing into the vapour phase. The up pointing hydrogen has no H bonding and is therefore not significantly red shifted from gaseous water stretching modes. The positive sign in the $\text{Im}\chi^{(2)}$ spectrum confirms the up pointing nature of this mode. The $\text{Im}\chi^{(2)}$ spectrum also shows a shoulder at around 2680 cm^{-1} with a positive sign for D_2O . Stiopkin and coworkers attribute this peak to a water molecule with two donor hydrogen bonds and one acceptor hydrogen bond.[1] Although this type of water molecule is oriented downwards, the positive sign can be linked to an antisymmetric linear combination of the two local modes caused by intramolecular coupling.[1] The origin of the two modes in the bonded OH frequency region ($3000 \text{ cm}^{-1} - 3500 \text{ cm}^{-1}$ for H_2O and $2250 \text{ cm}^{-1} - 2600 \text{ cm}^{-1}$ for D_2O) are debated. The 3200 cm^{-1} band (2350 cm^{-1} for D_2O) is often assigned to symmetric OH stretching of tetrahedrally hydrogen bonded water (icelike water). This peak shows a negative contribution to the $\text{Im}\chi^{(2)}$ spectrum.[27] The broad negative peak at around 3450 cm^{-1} is often attributed to symmetric stretching of asymmetrically hydrogen bonded water (liquidlike water).[27] However, in more a more recent study Schäfer and coworkers assign the double peak feature of the air-water interface to intramolecular Fermi resonance coupling of the OH stretch mode with an HOH bending overtone, while intermolecular coupling causes a red shift in the OH stretch response.[28] This is confirmed with isotopic dilution studies, where the 3200 cm^{-1} peak disappears for 50% dilution, because the HOD molecules have different coupling.[28]

Table 2.3: Signs of molecular susceptibilities of DAA and DDA-type water molecules.[3]

	DAA			DDA		
						
Mode	Bend	H-Bond OH	Free-OH	Bend	Sym. Str.	Antisym. Str.
Sign	-	-	+	+	-	0

The relationship between the sign in the $\text{Im}\chi^{(2)}$ and the orientation of the transition dipole moment is mode dependent. The typical conformations at the water-air interface are DAA (or DA), with one donating hydrogen bond and DDA with two donating hydrogen bonds. Since the hydrogen bonded OH (3510 cm^{-1}) and the free-OH (3700 cm^{-1}) stretching modes have different energies, the vibrational modes are de-coupled and the transition dipole moments are therefore parallel to the bond direction.[1][3] For these decoupled modes a negative (positive) sign can be directly translated into a down (up) orientation. For the bending mode this picture is not as simple, but in table 2.3 the direction of the transition dipole is assumed to be parallel to the angular bisector. However, simulations of SFG spectra reveal an opposite sign of the transition polarizability than for the bending modes, where the sign is positive despite the orientation. This leads to a negative (positive) sign for the bending mode corresponding to a up (down) orientation. For the DDA water molecules it is assumed that both hydrogen bonds are of equal strength. Here, both bonds are coupled and therefore the direction of the transition dipole moment for the symmetric (antisymmetric) OH stretch mode is parallel (perpendicular) to the angular bisector instead of the bond directions. When the angular bisector is parallel to the surface normal the symmetric stretch mode is SFG active and the antisymmetric stretch mode is inactive.[3]

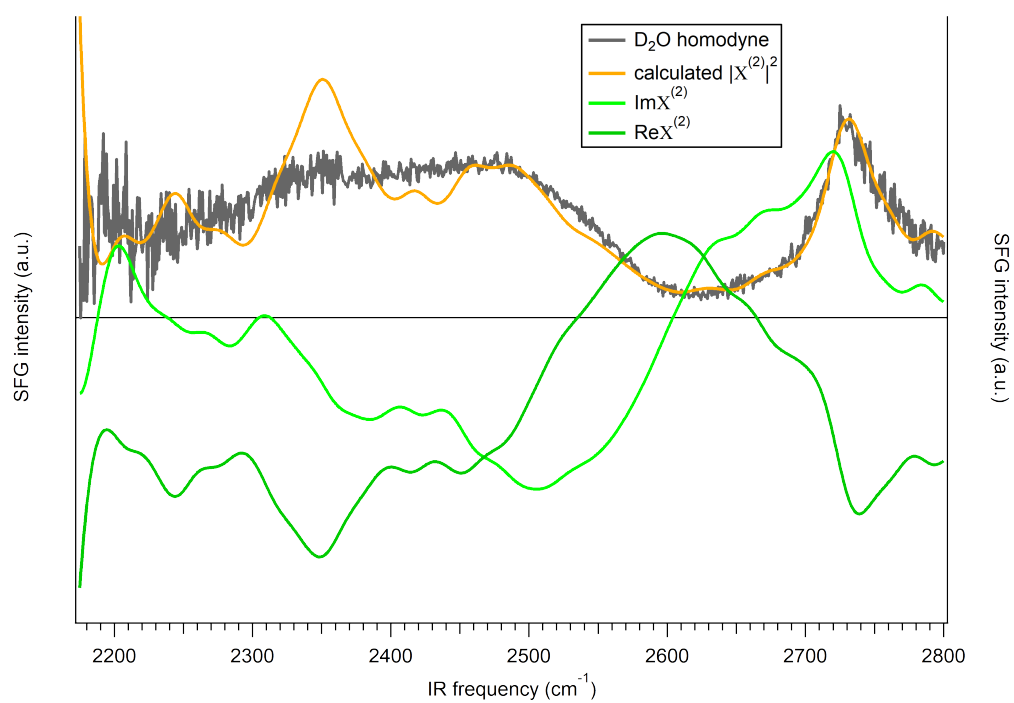


Figure 2.15: Direct and phase-sensitive SFG spectra at the D₂O-air interface.

Chapter 3

Results and Discussion

The effects of nonionic surfactant mixtures have been investigated by tensiometry and direct and phase-sensitive vibrational sum frequency generation spectroscopy. The results are presented in this chapter.

3.1 Tensiometry

Surface pressure measurements were conducted, because they are a good first indicator to study, whether surfactants are located at the air-water interface, as seen in equation 2.15.

The setup was first normalised to neat water and afterwards exchanged for a surfactant solution. The height of the probe above the surface and therefore the size of the meniscus were held as consistent as possible. Nevertheless because the needle of the tensiometer has to be reapplied to the surface after exchanging the water, this introduces an inherent error. This error was corrected by reapplying the needle multiple times and taking an average value.

Figure 3.1 shows surface pressure measurements of mixtures between aqueous dodecanol and dodecylamine solutions with a total surfactant concentration of $c = 2 \times 10^{-8}$ mol/mL. Mixtures are represented by their mole fraction of dodecanol $x(\text{DOH})$.

The different solutions show varying behaviour over time. For dodecanol after each reapplication of the needle, a drop in surface pressure was observed, followed by an increase and then a saturation. For dodecylamine, after the reapplication of the needle, a drop in surface pressure was also observed. But here it is followed by a sharp increase and then a slow decrease followed by saturation. The $x(\text{DOH}) = 0.25$ and $x(\text{DOH}) = 0.75$ mixtures do not show an equilibration over time. The $x(\text{DOH}) = 0.50$ mixture shows a rather quick equilibration.

Besides the error arising from differing height of the probe, evaporation may cause inconsistencies in the measurement. The presence of surfactants lowers the surface tension and therefore increase the evaporation rate.[29] This could be improved by using a lid and therefore limit the evaporation.

Because of the inherent error the average values for the surface pressure shown in figure 3.2, the absolute values should only be compared to other literature values with reservations. Nevertheless since the procedure for all the mixtures is the same, the general trend is convincing. The error shown in figure 3.2 is the standard deviation.

Generally one can see a trend that the pure surfactant solution have a lower surface pressure than the mixtures; a maximum surface pressure is reached at the 50:50 mixture. This trend is in line with studies conducted by Fauser and coworkers with charged surfactant mixtures (see figure 3.2 b)).[5] Figure 3.2 b) shows surface tension measurements plotted against the mixing ratio of sodium dodecylsulfate (SDS) and dodecyltrimethylammonium bromide (C_{12}TAB) in different total surfactant concentrations.[5] SDS and C_{12}TAB have similar charge densities and only differ in polarity, with SDS being negatively and C_{12}TAB being positively charged. At the shown concentrations the pure surfactant solutions show no noticeable surface activity ($\gamma_{\text{water}} = 72.7$ mN/m at

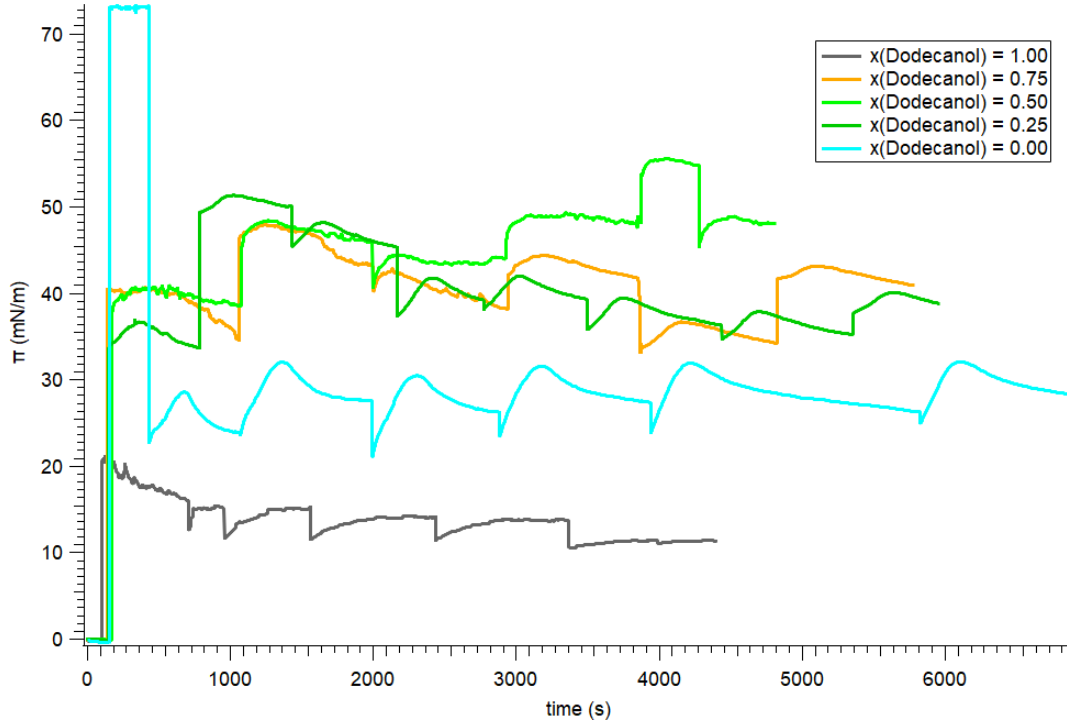


Figure 3.1: Surface pressure measurements of mixtures of aqueous dodecanol and dodecylamine solutions with a total surfactant concentration of $c = 2 \times 10^{-8}$ mol/mL and pH 11.

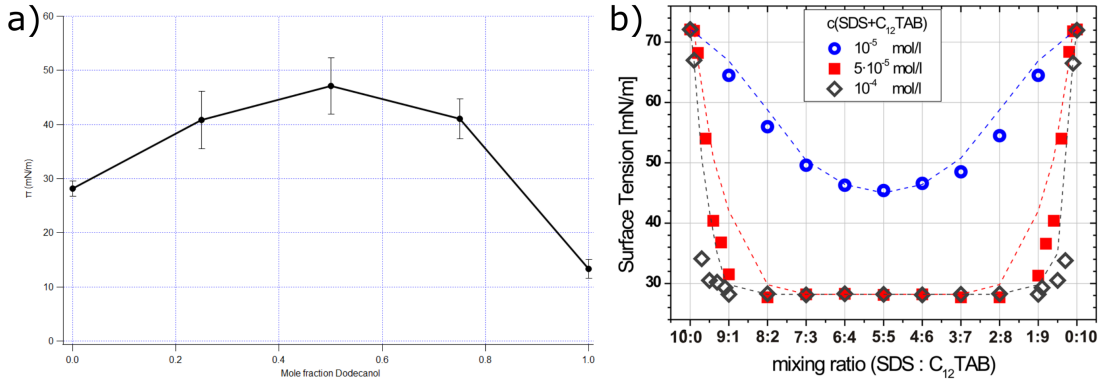


Figure 3.2: a) Surface pressure plotted against mole fraction of dodecanol $x(\text{DOH})$. b) Surface tension measurements of SDS/ C_{12}TAB mixtures taken from Fauser and coworkers.[5]

293 K [30]). The pure surfactants only show a decrease in surface tension starting from a bulk concentration of $c = 1 \times 10^{-3}$ mol/mL.[5] Fauser and coworkers found for all used concentrations that the surface tension decreases, and therefore the surface pressure increases, for surfactant mixtures. For total concentrations above 5×10^{-8} mol/L there is a plateau from roughly 8:2 to 2:8 mixing ratio at 28 mN/m. For higher concentrations of the neat surfactants the minimum surface tension reached is 38 mN/m. This suggests a synergistic effect which favours the adsorption of catanionic mixtures. Fauser et al. explain this synergistic behaviour with the formation of catanionic complexes where the SDS and C_{12}TAB molecules are ionically bonded at the head groups. These complexes are charge neutral and the weaker electrostatic repulsion allows for a

more densely packed monolayer.[5]

In the data presented in this work the synergistic effect in adsorption is also present, but because mixtures of nonionic surfactants were used the origin of this effect is not necessarily the same. It is, however, possible that, through hydrogen bonding, these head to head complexes do form, but it is likely that they show a weaker bonding than the coulomb bonded catanionic complexes.

3.2 SFG Spectroscopy

3.2.1 CH Stretch Domain

In order to further investigate the effects of surfactant mixtures on surfactant conformations at the air-water interface, SFG experiments were conducted. Figure 3.3 a) shows SFG spectra in the CH stretch frequency domain over time with different mixtures of dodecylamine and dodecanol. A rotating trough was used. All samples have a pH=11, through added KOH, to ensure that dodecylamine is not protonated.

The coloured boxes show the range over which the peaks were integrated in figures 3.3 b-d). For the integration a baseline was subtracted. Table 3.1 shows the assignment of the peaks in the CH domain with their respective standard deviations. For all spectra there was no major shift in peak positions, which is to be expected since dodecanol and dodecylamine have the same C12 tailgroup and only differ by the headgroup. The peak around 2860 cm^{-1} can be assigned to the CH_2 symmetric stretching mode d^+ , the peak around 2890 cm^{-1} stems from the CH_3 symmetric stretching mode r^+ and the broad peak at around 2955 cm^{-1} can be attributed to two peaks, one being the Fermi resonance of the CH_3 symmetric stretch mode r^+ and the other being the asymmetric stretching mode of CH_3 r^- . The two modes contributing to the 2955 cm^{-1} peak explains the different shape of the peak and the heterodyne spectra shown in section 3.2.3 further verify this assumption.[31]

Table 3.1: Peak assignment.

x(DOH)	Wavenumber (cm^{-1})		
	d^+	r^+	r_{FR}^+ and r^-
0.00	2860 ± 1	2889 ± 1	2955 ± 1
0.25	2860 ± 1	2888 ± 1	2951 ± 6
0.50	2858 ± 2	2888 ± 0	2954 ± 1
0.75	2860 ± 1	2890 ± 1	2954 ± 1
1.00	2863 ± 0	2893 ± 1	2960 ± 1

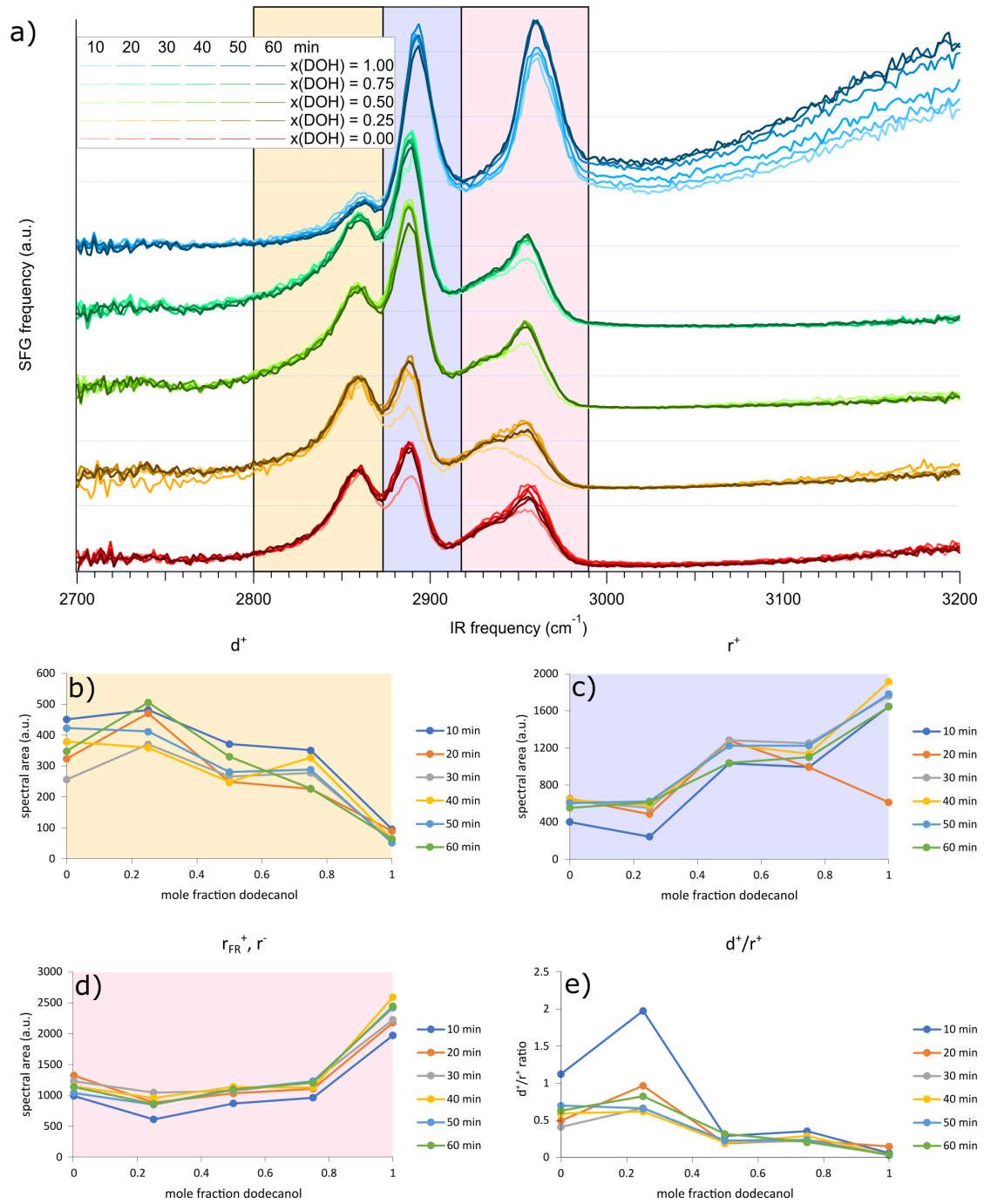


Figure 3.3: a) SFG spectra over time with different mixtures of dodecylamine and dodecanol. The total surfactant concentration is $c = 2 \times 10^{-8}$ mol/mL and is displayed as the mole fraction x of dodecanol. The coloured boxes indicate the range over which the peaks were integrated. The different mixtures are offset for better visualization and the time is indicated by the brightness of the colors used. b) d^+ peak area plotted against mole fraction of dodecanol. c) r^+ peak area plotted against mole fraction x of dodecanol. d) r_{FR}^+ and r^- peak area plotted against mole fraction x of dodecanol. e) d^+/r^+ peak area ratio plotted against mole fraction x of dodecanol.

Figure 3.3 b) shows a plot of the spectral area of the CH_2 symmetric stretch peaks against the mole fraction $x(\text{DOH})$ of dodecanol. A trend is visible, where there is a decrease in spectral area with increasing $x(\text{DOH})$. The pure dodecanol solution has the lowest intensity. Figure 3.3 c) shows the spectral area of the symmetric stretch CH_3 peaks plotted against the mole fraction of dodecanol $x(\text{DOH})$. Here an opposite trend from the symmetric stretch CH_2 peaks is present, where there is an increase in spectral area with increasing mole fraction of dodecanol $x(\text{DOH})$. Figure 3.3 d) shows the plot of the integrated spectral area of the symmetric stretch CH_3 Fermi resonance, as well as the antisymmetric stretch CH_3 peaks. Here, with increasing mole fraction of dodecanol $x(\text{DOH})$ there is first a decrease followed by an increase in spectral area. The lowest point is at $x(\text{DOH}) = 0.25$ and pure dodecanol has the highest intensity.

From the intensity of the CH_2 and the CH_3 symmetric stretch peaks conclusions about the orientation of the surface molecules can be drawn. Surfactants orient in a way at the surface where the hydrophilic head-group is forming hydrogen bonds with water molecules and the hydrocarbon tail is pointing away from the surface. In a liquid condensed monolayer (LC), where the surfactants are stacked and highly ordered, most of the CH_2 groups are in a local centrosymmetric medium and therefore do not generate a SFG signal.[15] On the other hand all the CH_3 groups are oriented similarly and are not in a local centrosymmetric environment and therefore generate a SFG signal. Furthermore if you consider a gaseous (G) - or liquid expanded monolayer (LE), the surfactants are not stacked and occupy a large area on the surface. The energy difference between trans and gauche conformation is 3.3 kJ/mol, which roughly corresponds to kT at room temperature.[15] This means in a low density monolayer there are both trans and gauche conformation in the surfactant hydrocarbon tails. Gauche defects towards the end of the chain cause CH_3 groups to be tilted towards the surface, which leads to the SFG signals to partially cancel out. Because of that the ratio between d^+ and r^+ spectral area can be used as an indicator of ordering within the monolayer.

Figure 3.3 e) shows the ratio between CH_2 and CH_3 spectral areas plotted against the mole fraction of dodecanol. Here one can see a clear trend where with increasing the mole fraction of dodecanol the ratio tends downwards and order increases. However the highest ratio is found at $x(\text{DOH}) = 0.25$.

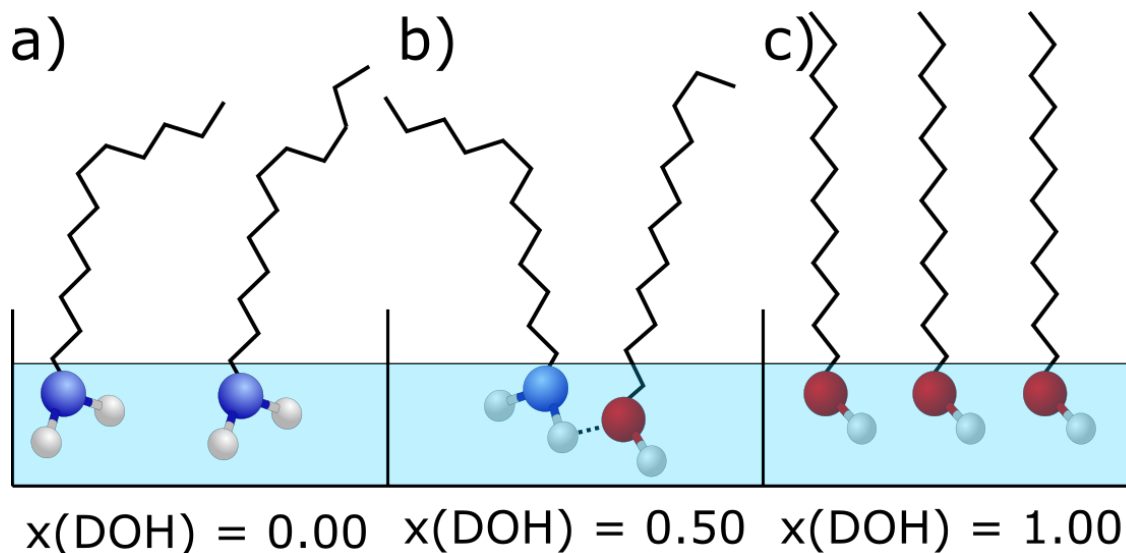


Figure 3.4: Schematic drawing of surfactants at the air-water interface. a) Dodecylamine b) 1:1 mixture of dodecylamine and dodecanol and c) dodecanol.

Figure 3.4 shows schematic drawings of surfactants at the air-water interface. Comparing pure dodecanol and dodecylamine, there is a higher d^+/r^+ ratio and therefore more gauche defects for dodecylamine than for dodecanol.

Since there still is d^+ signal present for dodecanol, the monolayer is not completely gauche defect free.

The higher d^+/r^+ ratio for the mixtures could point to hydrogen bonded complexes similar to the catanionic surfactant complexes described by Fauser and coworkers are schematically shown in figure 3.4 b) and could cause a more densely packed monolayer to form compared to pure dodecylamine.[5] These surfactant complexes could also explain the increased surface pressure found for, these mixtures, with a synergistic adsorption to the air water interface.

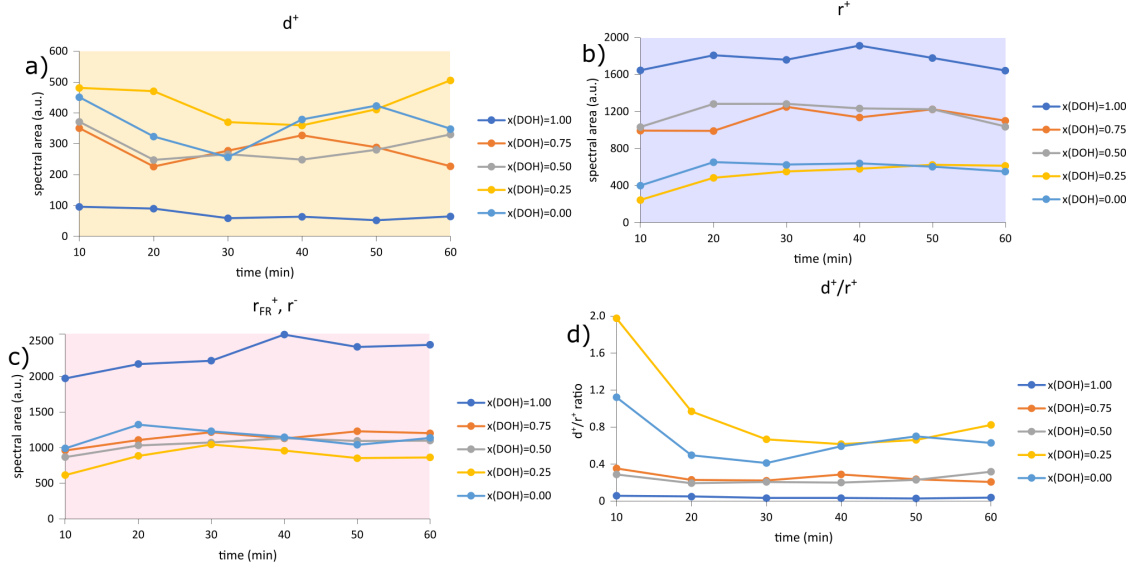


Figure 3.5: a) d^+ peak area plotted against time. b) r^+ peak area plotted time. c) r_{FR}^+ and r^- peak area plotted against time. d) d^+/r^+ peak area ratio plotted against time.

Figure 3.5 a) shows the integrated spectral area of the CH_2 symmetric stretch peak plotted against time. For pure dodecanol the intensity decreases over time and then stabilizes. For all other spectra the CH_2 intensity fluctuates over time. Figure 3.5 b) shows the integrated spectral area of the CH_3 symmetric stretch peak plotted against time. All spectra show an increase in the beginning and a stabilization over time. Figure 3.5 c) shows the integrated spectral area of the CH_3 symmetric stretch Fermi resonance peak and the CH_3 asymmetric stretch peak plotted against time. For all spectra there is an increase of intensity at the start and then a stabilization over time. Figure 3.5 d) shows the ratio between CH_2 and CH_3 integrated spectral areas plotted against time. The ratio for all spectra is decreasing at the start and then stabilizing over time. This means that the ordering of the adsorbed monolayer increases over time until the monolayer is fully stabilized.

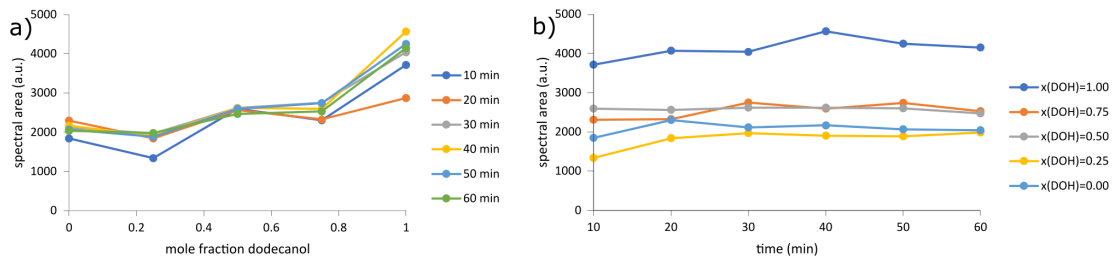


Figure 3.6: Total spectral area of all CH peaks plotted against a) mole fraction $x(\text{DOH})$ of dodecanol and b) time.

Figure 3.6 a) shows the total spectral area integrated over all CH peaks plotted against the mole

fraction of dodecanol. The spectral area increases with higher mole fraction of dodecanol for dodecanol-dodecylamine mixtures. Figure 3.6 b) shows the total integrated spectral area plotted against time. For all samples but the $x(\text{DOH}) = 0.50$ the spectral area increases over time and then stabilizes. The 1:1 mixtures is stable over time.

3.2.2 Bonded OH Domain

Figure 3.7 a) shows a SFG spectrum of dodecylamine in water at pH 11 with a concentration of 2×10^{-8} mol/mL (0.02 mM). Figure 3.7 b) shows a SFG spectrum taken from Nguyen and coworkers of 1 mM dodecylamine hydrochloride (DAH).[32] Besides the differing concentrations the main difference between the DAH spectrum in b) and dodecylamine spectrum in a) is the difference in pH, which suggests a different protonation state of amine. This can explain the sharp peak at 3080 cm^{-1} in figure 3.7 b). Therefore it is likely that this peak stems from a N^+H vibration. The peak at around 3200 cm^{-1} originates most likely from interfacial water, since this peak is present in both the protonated and the non-protonated spectrum. Also a peak at around 3400 cm^{-1} is present in both spectra and probably also stems from interfacial water. Finally the deprotonated spectrum a) shows a peak at around 3300 cm^{-1} , which is missing from the protonated spectrum in b), and can therefore be assigned to a NH vibration.[32]

Figure 3.7 c) shows SFG spectra taken from Nguyen and coworkers[32] of 0.0025 mM hexadecylamine (HAD) in saturated salt solution with no pH control and 0.005 mM hexadecylamine (HAD) in water with no pH control. The purpose of the salt solution is to suppress signal coming from the response of water molecules in near bulk region (so called $\chi^{(3)}$ response). The charged surfactants induce a surface potential and the resulting \vec{E} -field breaks the symmetry over a long range. Adding salt to the solution introduces a oppositely charged layer, which shields the surface charge and shortens the range of the \vec{E} -field.[33] The 3200 cm^{-1} and 3400 cm^{-1} peaks are largely suppressed and only the 3080 cm^{-1} peak is unchanged. This further shows that only the 3080 cm^{-1} peak comes from the N^+H vibration and the other peaks come from interfacial water.[32]

Comparing the spectrum in figure 3.7 with the assignment of the peaks in the neat water spectrum (see section 2.4.2) the two peaks stemming from interfacial water are roughly in the same position as for neat water. Therefore these peaks can be assigned according to table 3.2. The FT-IR spectrum of dodecylamine shows a symmetric NH stretch mode at 3177 cm^{-1} and an asymmetric NH stretch mode at 3285 cm^{-1} . [34] Slight shifts are to be expected and therefore the peak at 3310 cm^{-1} most likely stems from NH asymmetric stretch vibrations. There is no peak around 3177 cm^{-1} but it is presumably because of the neighbouring symmetric stretch OH peak masking the NH symmetric stretch mode. There is a higher intensity for the 3200 cm^{-1} bonded OH stretch peak than the 3430 cm^{-1} bonded OH stretch peak, while for neat water both have similar intensities. This could also be explained by the masked NH symmetric stretch peak contribution.

The SFG spectra presented in figure 3.8 were taken from a different SFG setup, as the previously shown spectra, that did not allow to utilize a rotating trough. Therefore the comparison with the previous experiment is not straight forward. If an inhomogenous monolayer would be present, the rotating trough would lead to an average over a large area of the surface, while the stationary trough would cause variance, depending on where the measurement was taken. Also not moving the laser spot around on the surface, can induce a flow away from the laser focus. For lower

t

Table 3.2: Peak assignment for dodecylamine in H_2O at pH 11.

Mode	Wavenumber (cm^{-1})
FR coupling of OH stretching and HOH bending overtone and N-H symmetric stretching	3200
N-H asymmetric stretching	3310
bonded OH symmetric stretching	3430

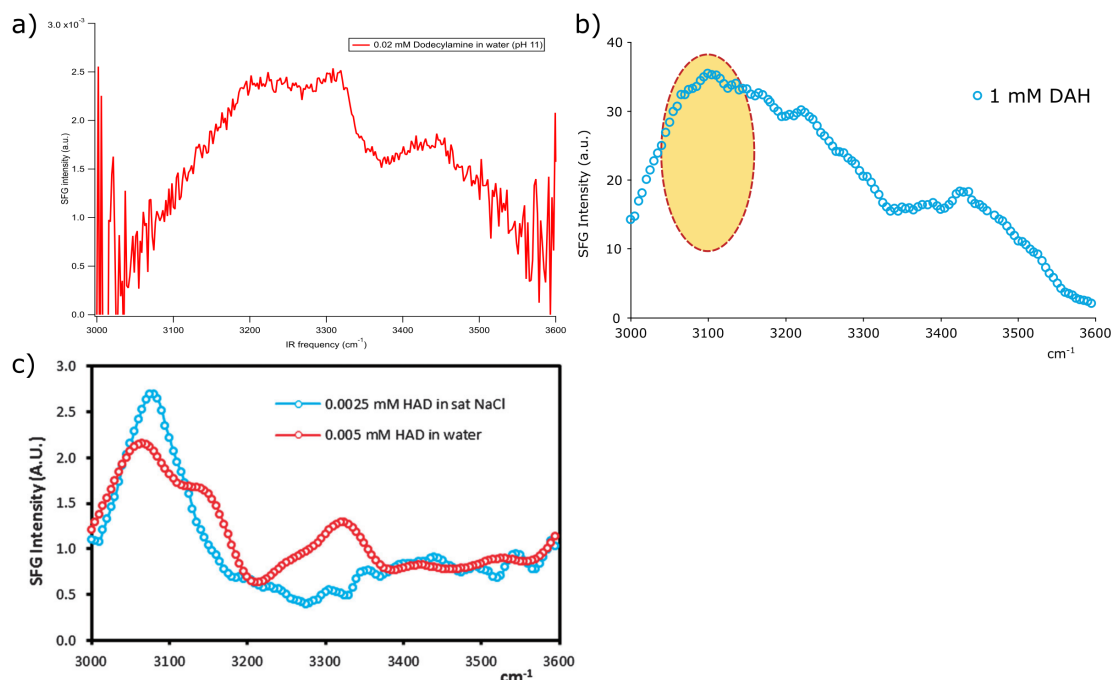


Figure 3.7: a) SFG spectrum of dodecylamine in water $c = 0.02$ mM at pH 11. b) SFG spectra of 1 mM dodecylamine hydrochloride (DAH) in water. c) SFG spectra of 0.0025 mM hexadecylamine hydrochloride (DAH) in saturated NaCl solution and 0.005 mM hexadecylamine hydrochloride (DAH) in water. Figures b) and c) was taken from Nguyen and coworkers.[32]

surfactant densities at the surface this flow may carry away surfactant molecules, which could lead to a diminishing SFG signal.[35] To limit this effect the trough was manually rotated before the measurement of each SFG spectrum.

Figure 3.8 a) shows average SFG spectra of different mixtures of dodecanol and dodecylamine with a total surfactant concentration of 2×10^{-8} mol/mL in an aqueous KOH solution with a pH of 11. The integrated peak areas for the bonded OH frequency domain are plotted against the mole fraction of dodecanol in Figure 3.8 b). For the integration a baseline was subtracted.

Comparing the spectra to figure 3.3 it can be seen that the bonded OH band is in both cases more intense for pure dodecanol, than for the other mixtures. The CH peak positions and magnitudes are also in line but are slightly shifted. This is probably an error in the calibration of the IR frequency in figure 3.3, since the position of CH peaks are closer to the literature value in this data set.

In bonded OH frequency domain, there is a nonlinear trend visible, where the pure substances show a more intense bonded OH band than the mixtures. This nonlinear trend is shown in figure 3.8 b) and is compared to a hypothetical linear trend. Figure 3.9 shows a schematic drawing of the proposed surface structure that may be responsible for the reduced SFG signal for dodecanol/dodecylamine mixtures. The two surfactants show different hydrogen bonding strength and therefore have different penetration depth into the water surface. If both surfactants are present the monolayer is no longer uniform in depth and has varying headgroup positions. This may introduce additional disorder to the hydrogen bonded water network and therefore reduce the SFG signal. This hypothesis, however, needs to be examined more thoroughly. The schematic drawing is not supposed to reflect a specific hydrogen bonding scheme but rather the general principle that surfactant mixtures have varying penetrating depth due to hydrogen bonding strength.

It has to be noted that the bonded OH band of dodecylamine has a different shape as in figure 3.7. The origin of the differing shape is unclear.

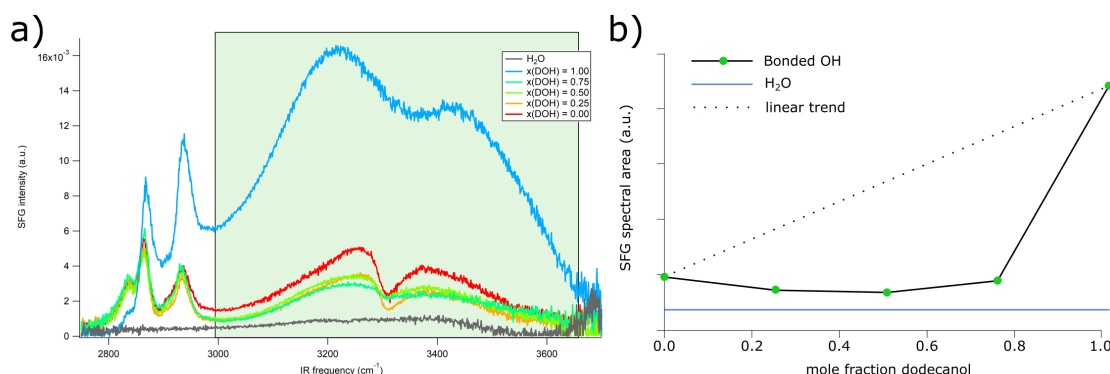


Figure 3.8: a) SFG spectra of different mixtures of dodecanol (DOH) and dodecylamine in water/KOH (pH 11) with a total surfactant concentration of 2×10^{-8} mol/mL. The coloured boxes indicate the integration range. b) Spectral area of the bonded OH region plotted against the mole fraction of dodecanol $x(\text{DOH})$. The dotted line represents a hypothetical linear trend for comparison. The reason for the differing shape of the dodecylamine spectrum is unclear.

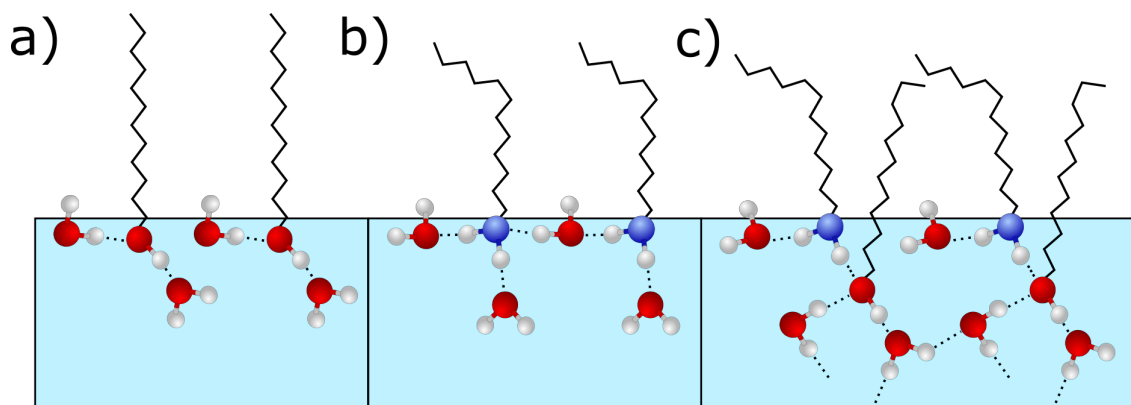


Figure 3.9: Proposed effect of surfactants on the water structure. a) Pure dodecanol, b) pure dodecylamine and c) one to one mixture of dodecanol and dodecylamine.

3.2.3 OD and CH Stretch Domain

Additionally to the experiments in H_2O , similar experiments were conducted in D_2O . The spectra shown were taken at the same SFG setup as the spectra shown in Figure 3.8 a), and therefore a rotating trough could not be used.

Figure 3.10 a)-e) shows SFG spectra of different mixtures of dodecanol and dodecylamine with a total surfactant concentration of 2×10^{-8} mol/mL in decreasing order of the mole fraction $x(\text{DOH})$ of dodecanol. For all mixtures a trend can be seen, where the intensity increases with time and then an equilibrium is reached. Figure 3.10 f-h) show the integrated spectral area of the symmetric stretch CH_2 (d^+), the integrated spectral area of the symmetric stretch CH_3 (r^+) and their ratios plotted against time. The d^+ spectral area for $x(\text{DOH})=0.75$ has a downward trend over time while the $x(\text{DOH})=0.50$ and $x(\text{DOH})=0.25$ mixtures increase with time. The r^+ spectral area increases over time for all mixtures. The d^+/r^+ ratio tends downwards over time and then stabilizes, which means that the number of gauche defects in the monolayer decreases over time. This is in line with the previous experiments. It has to be noted that for $x(\text{DOH}) = 0.00$ - $x(\text{DOH}) = 0.75$ the monolayer did not seem to be homogeneous, because on some laser focus positions there was a very weak CH signal or the signal was indistinguishable from the D_2O spectrum (see figure 3.10 c) and d)). By changing the position a higher signal could be achieved.

A rotating trough would include these spots in the average. This can explain differences between measurements with and without a rotating trough.

After a certain time these spots with no intensity decreased in prevalence.

Table 3.3: Assignment of the CH peaks in the D₂O spectra.

$x(\text{DOH})$	Wavenumber (cm ⁻¹)		
	d ⁺	r ⁺	r _{FR} ⁺ and r ⁻
0.00	2834±3	2864±2	2924±11
0.25	2839±1	2865±1	2916±8
0.50	2838±1	2866±2	2917±1
0.75	2841±2	2866±2	2915±2
1.00	2838±2	2867±3	2913±5

Table 3.3 shows the assignment of the CH peaks in the D₂O spectra. The peak at 2717 cm⁻¹ for all mixtures is slightly shifted from free-OD in the pure D₂O spectrum (2728 cm⁻¹). Nevertheless this peak most likely stems from a free-OD vibration, where the free OD interacts weakly with the hydrocarbon chain, via Van der Waals interaction.

Alternatively this peak, might also be a CH₃ asymmetric bending overtone, which has been reported at 2755 cm⁻¹ for methane chemisorbed to the Pt(111) surface.[36] For a harmonic oscillator an overtone, which is a $\Delta v = 2$ transition, is a forbidden transition. The asymmetry of the potential for an anharmonic oscillator, which is a better model for molecular vibrations, violates that rule. Nevertheless the $\Delta v = 1$ still make up the vast majority of transitions. Therefore a CH bending overtone peak would be very weak.[2]

Furthermore the CH bending overtone would not be affected by changing the solvent from D₂O to H₂O, which would mean such a peak would also be expected in the H₂O spectra in Figure 3.3. There is however no such peak visible in the 2700 - 2800 cm⁻¹ range. The free-OH peak is shifted in the H₂O spectra to around 3700 cm⁻¹, and is therefore out of range of these spectra. For these reasons it can be assumed that this peak arises from free-OH interacting weakly with the hydrocarbon tail of the monolayer.

Figure 3.11 shows SFG spectra of different mixtures of dodecanol and dodecylamine solutions in D₂O with a pH of 11 and neat D₂O. The total surfactant concentration is $c = 2 \times 10^{-8}$ mol/mL. Figure 3.11 b)-g) show the b) d⁺ peak area, c) r⁺ peak area, d) r_{FR}⁺ and r⁻ peak area and e) d⁺/r⁺ peak area ratio plotted against mole fraction $x(\text{DOH})$ of dodecanol.

The d⁺/r⁺ ratio displayed in figure 3.11 shows a decrease with increasing mole fraction of dodecanol. Comparing figures 3.11 b)-e) with figures 3.3 b)-e) it can be seen that all figures show the same trend against the mole fraction of dodecanol, as in the previous experiment.

Figure 3.12 a) shows the bonded OD peak area and b) shows the free OD peak area plotted against mole fraction $x(\text{DOH})$ of dodecanol. The bonded OD region shows the same trend, as the bonded OH region in the previous experiment, where the neat surfactants have a higher spectral area than the surfactant mixtures. For all mixtures the bonded OD intensity is enhanced compared to neat water (blue line).

The free OD spectral area decreases with increasing mole fraction of dodecanol in a nonlinear fashion. This is in line with the previous findings. The d⁺/r⁺ ratio decreases in a similar fashion. This shows that with increasing the mole fraction of dodecanol the monolayer gets more densely packed which in turn means there are less water molecules with a free-OD and therefore the signal goes down. For all samples the free-OD signal is weaker than for neat water. This also makes sense since the neat water surface is not covered with surfactants and therefore show more water molecules with a free OD.

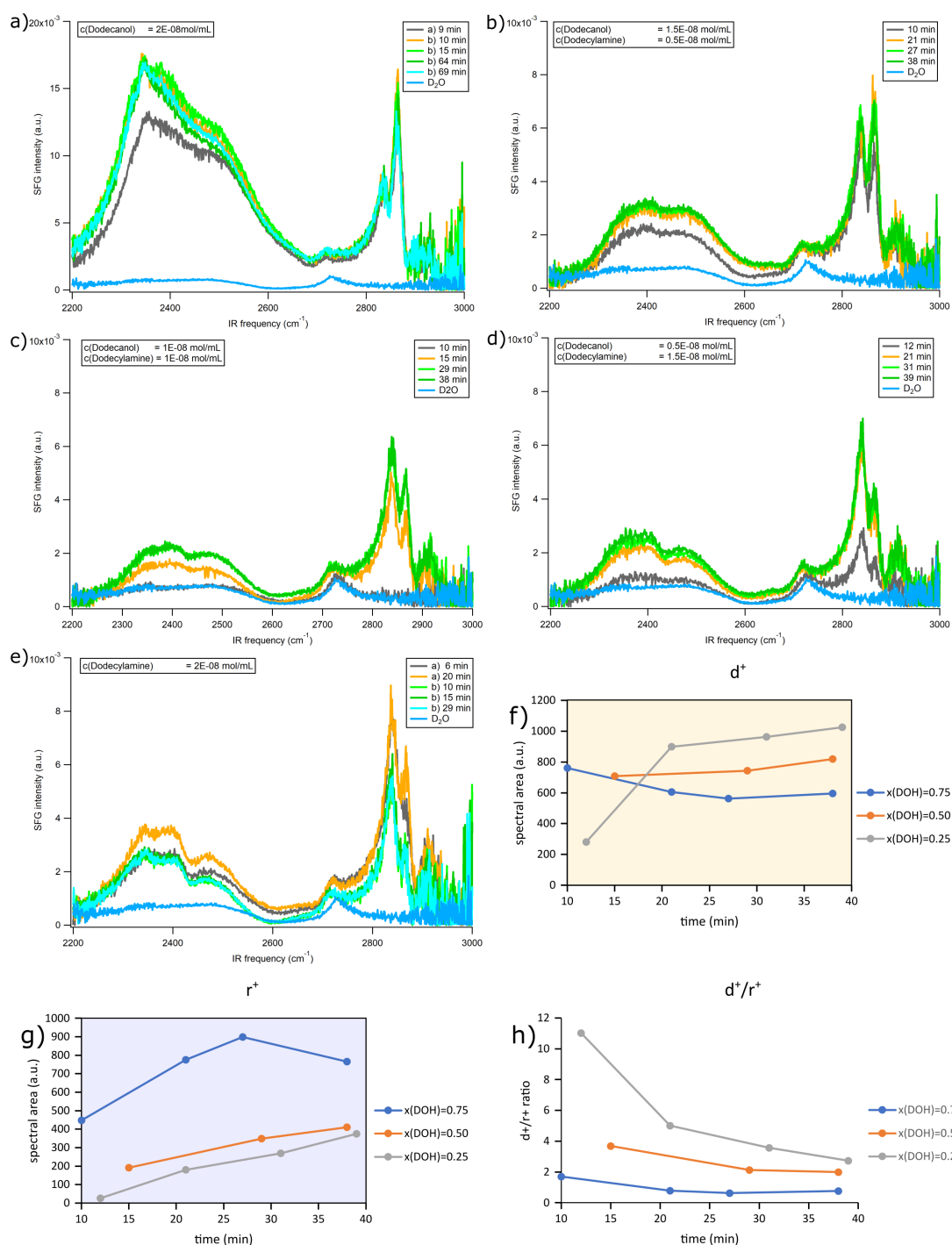


Figure 3.10: a) SFG spectra with $x(\text{DOH}) = 1.00$ in D₂O in the OD/CH domain. The two series a and b are from different samples. b) SFG spectra with $x(\text{DOH}) = 0.75$ in D₂O in the OD/CH domain. c) SFG spectra with $x(\text{DOH}) = 0.50$ in D₂O in the OD/CH domain. d) SFG spectra with $x(\text{DOH}) = 0.25$ in D₂O in the OD/CH domain. e) SFG spectra with $x(\text{DOH}) = 0.00$ in D₂O in the OD/CH domain. The two series a and b are from different samples. f) Integrated spectral area of the symmetric stretch CH₂ peak (d^+) plotted against time. g) Integrated spectral area of the symmetric stretch CH₃ peak (r^+) plotted against time. h) Ratio of the d^+ and r^+ spectral area plotted against time.

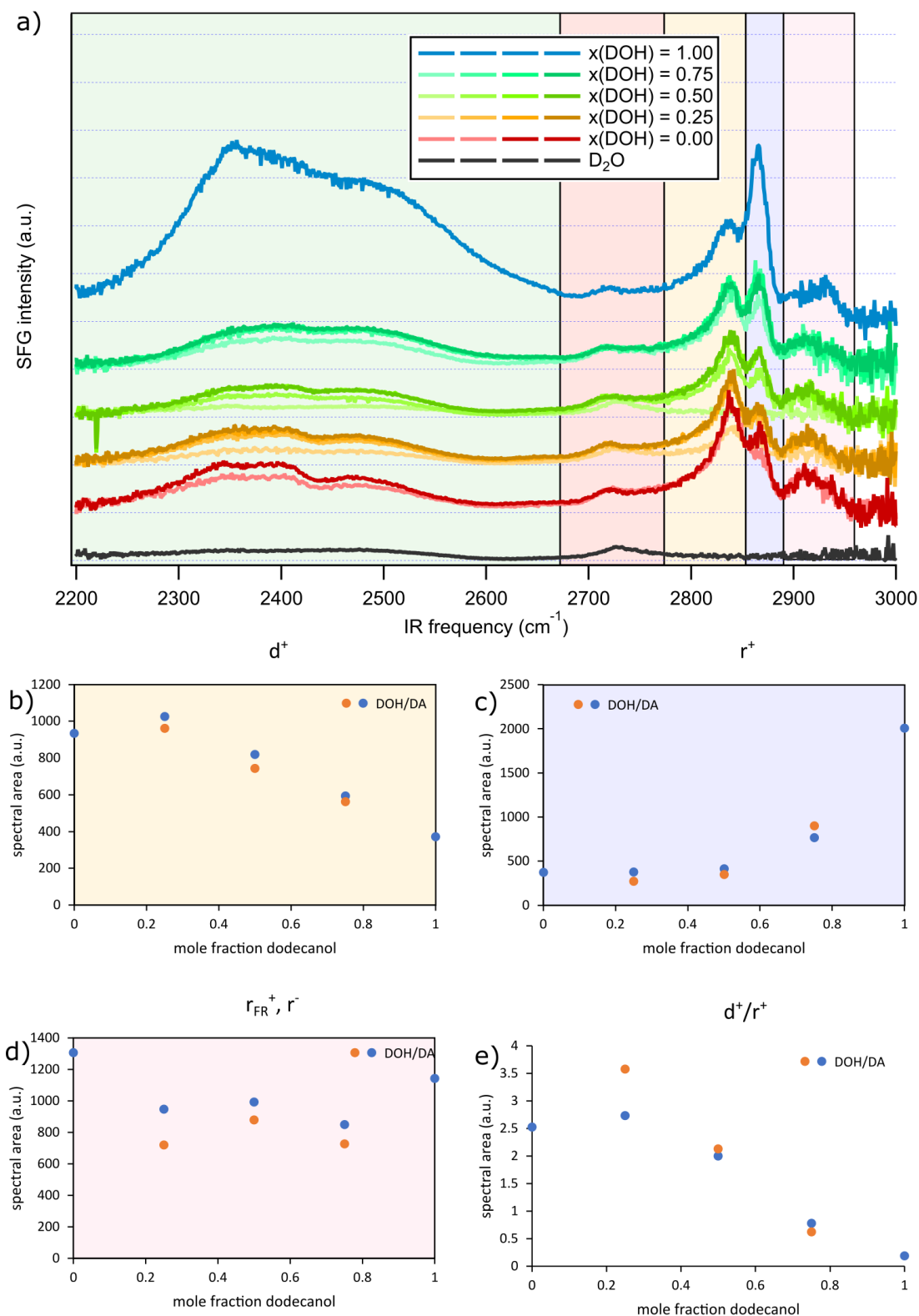


Figure 3.11: a) SFG spectra over time with different mixtures of dodecylamine and dodecanol in D_2O at a pH of 11. The total surfactant concentration used is $c = 2 \times 10^{-8}$ mol/mL and is displayed as the mole fraction x of dodecanol. The coloured boxes indicate the range over which the peaks were integrated. b) d^+ peak area, c) r^+ peak area, d) r_{FR}^+ and r^- peak area, e) d^+/r^+ peak area ratio.

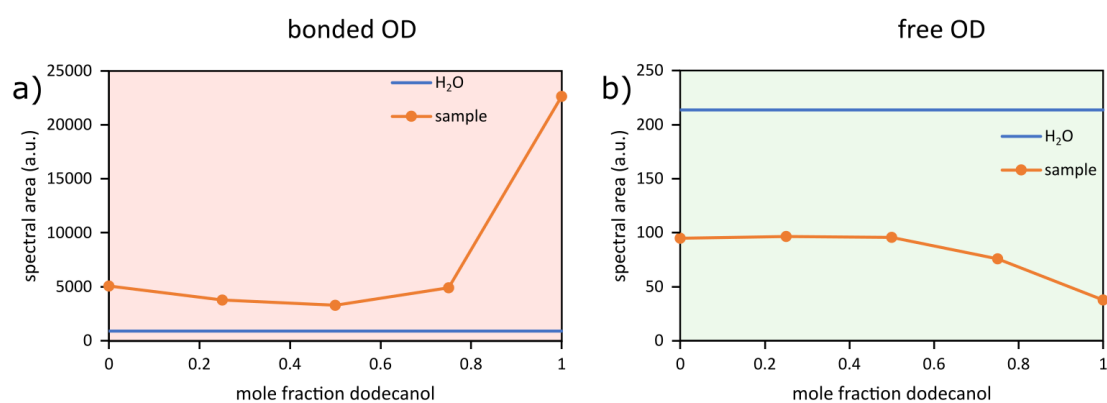


Figure 3.12: a) Bonded OD peak area and b) free OD peak area plotted against mole fraction $x(\text{DOH})$ of dodecanol.

3.2.4 Phase-sensitive SFG

Phase-sensitive SFG (PS-SFG) spectra can reveal the absolute orientation (up or down) of the molecules at the interface.[37] Figure 3.13 and 3.17 show the direct SFG spectra as well as the calculated $|\chi^{(2)}|^2$ spectrum. The real and imaginary part of the complex $\chi^{(2)}$ spectrum are displayed separately.

The calculated $|\chi^{(2)}|^2$ spectrum can be used to check the phase correction of the phase-sensitive SFG spectra. A close relationship between calculated and measured $|\chi^{(2)}|^2$ spectra, if measured directly after one another, means that the phase correction was done correctly.

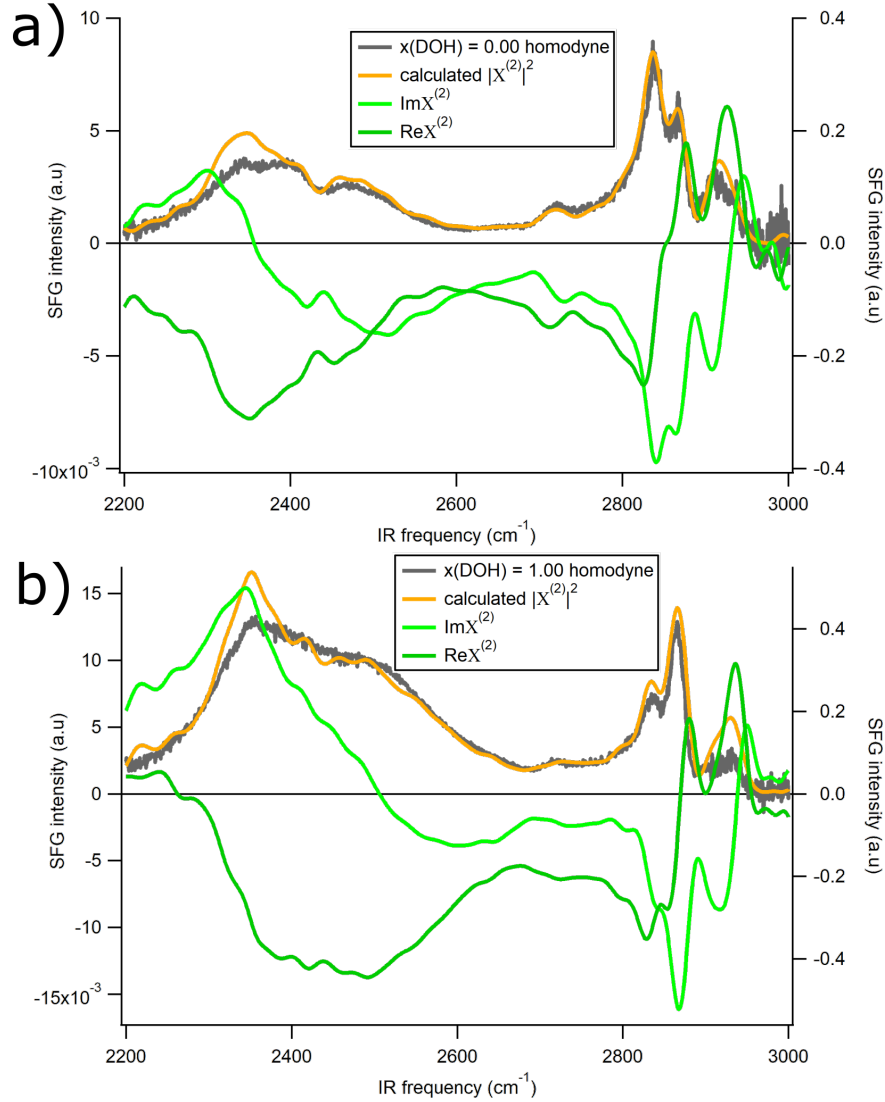


Figure 3.13: Direct and phase-sensitive SFG spectra at the D₂O-air interface of a) dodecylamine and b) dodecanol solutions with $c = 2 \times 10^{-8}$ mol/mL and a pH of 11.

Figure 3.13 a) shows the direct and phase-sensitive spectra of dodecylamine. The three peaks visible in the bonded OD region show different signs in the $\text{Im}\chi^{(2)}$ spectrum. The peak at around 2340 cm^{-1} has a positive sign and the peaks at around 2400 cm^{-1} and 2470 cm^{-1} have a negative sign. The negative sign of the 2400 cm^{-1} peak is to be expected, if the peak arises from a ND stretch vibration, because the dodecylamine molecules are down oriented.

Figure 3.14 shows the orientation of water molecules and their respective signs in the $\text{Im}\chi^{(2)}$

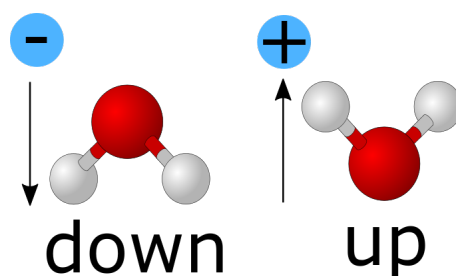


Figure 3.14: Schematic drawing of the orientation of water molecules and the corresponding sign in the $\text{Im}\chi^{(2)}$ spectrum.[22]

spectrum.

The 2470 cm^{-1} peak has the same sign as in the neat D_2O spectrum (figure 2.15), but the sign of the 2340 cm^{-1} peak is positive and therefore reversed. The signs of these peaks seem to be the same for all mixtures of dodecanol and dodecylamine. The 2400 cm^{-1} peak gets weaker with decreasing mole fraction of dodecylamine until it disappears completely for pure dodecanol. This further proves the assignment of this peak to a ND stretch vibration. The flipped sign for the 2340 cm^{-1} peak could hint on a change of the water structure at the interface, where one water molecule is flipped due to interaction with the surfactant head group.

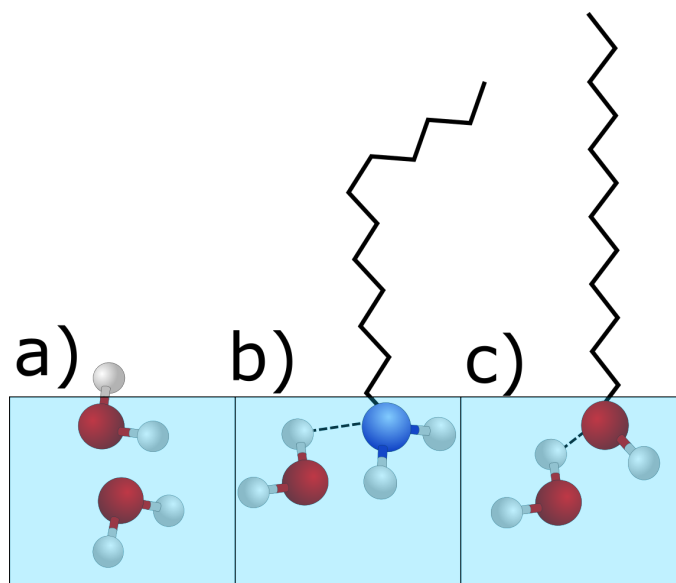


Figure 3.15: Schematic drawing of water molecules in the surface layer for a) pure water, b) dodecylamine hydrogen bonding to water and c) dodecanol hydrogen bonding to water.

Figure 3.15 shows a proposed schematic drawing of the ordering effect that surfactants have on surface water molecules. Figure 3.15 a) shows two water molecules where one is oriented up and one is oriented down. Since the up oriented water has a free OH mode the frequency is shifted and therefore does not contribute to the bonded OH. The hydrogen bonding between a water molecule and the surfactant head groups shown in figure 3.15 b) and c) is similar enough to the water-water hydrogen bonding for the vibration mode to contribute to the bonded OH spectrum. This flip of a water molecule would explain the positive sign for the 2340 cm^{-1} mode as the flipped water has the same orientation as the free OH.

The magnitude of the 2340 cm^{-1} peak is more than double for pure dodecanol (figure 3.13 b)) than for dodecylamine (figure 3.13 a)) and the dodecanol dodecylamine mixtures (figure 3.17

a)-c)). This shows that dodecanol has a stronger ordering effect on the surface water molecules due to stronger hydrogen bonding. The hydrogen bonding strength between alcohols and water is very similar to that of water and water, because of very similar electronegativity differences.[38] Amines have a smaller electronegativity difference and therefore form weaker hydrogen bonds with water.

For the mixtures the magnitude of the 2340 cm^{-1} peak increases with higher mole fraction of dodecanol $x(\text{DOH})$.

The free OD range shows a positive peak for all spectra which is in line with its assignment as a slightly shifted free OD peak.

In the CH stretch domain the symmetric stretch CH_2 (d^+), symmetric stretch CH_3 (r^+) and symmetric stretch Fermi resonance (r_{FR}^+) have a negative sign, while the asymmetric stretch CH_3 peak (r^-) has a positive sign. This is in line with other studies on different hydrocarbon containing surfactants and confirms the phase correction.[30][39]

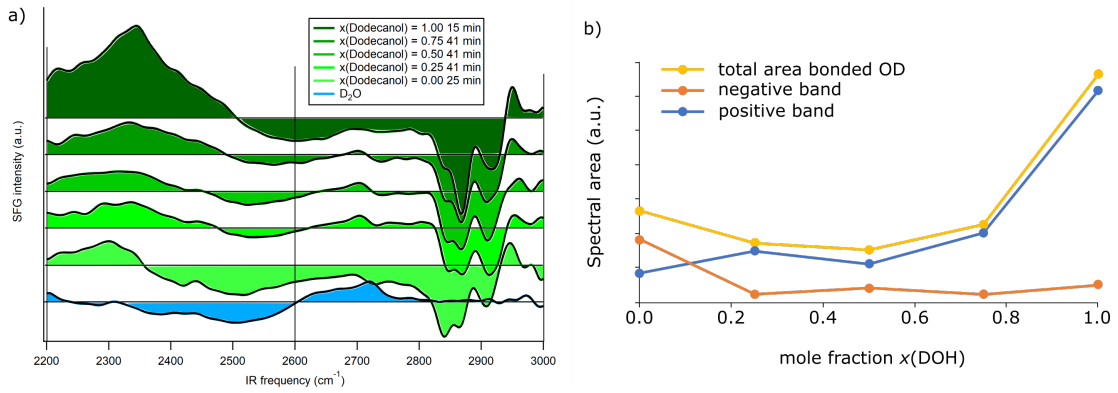


Figure 3.16: a) $\text{Im}\chi^{(2)}$ spectra of different mixtures of dodecanol and dodecylamine in D_2O with a total surfactant concentration of $c=2\times 10^{-8}\text{ mol/mL}$ and neat D_2O . The bonded OD frequency region ($2200\text{ cm}^{-1} - 2600\text{ cm}^{-1}$) was integrated and the positive and the negative bands were plotted separately and summed up against the mole fraction of dodecanol in b).

Figure 3.16 a) displays phase-sensitive $\text{Im}\chi^{(2)}$ spectra with the area under the curve coloured in. The bonded OD frequency region was integrated and the positive and the negative band were plotted separately and summed up against the mole fraction of dodecanol in figure 3.16 b). The total area of the bonded OD region is dominated by the positive band for all samples except pure dodecylamine, where the negative band has a larger contribution. The total peak area shows a nonlinear trend, where the mixtures have a lower spectral area than the neat surfactants and dodecanol has a higher spectral area than dodecylamine. This is the same trend as seen in the previous experiments.

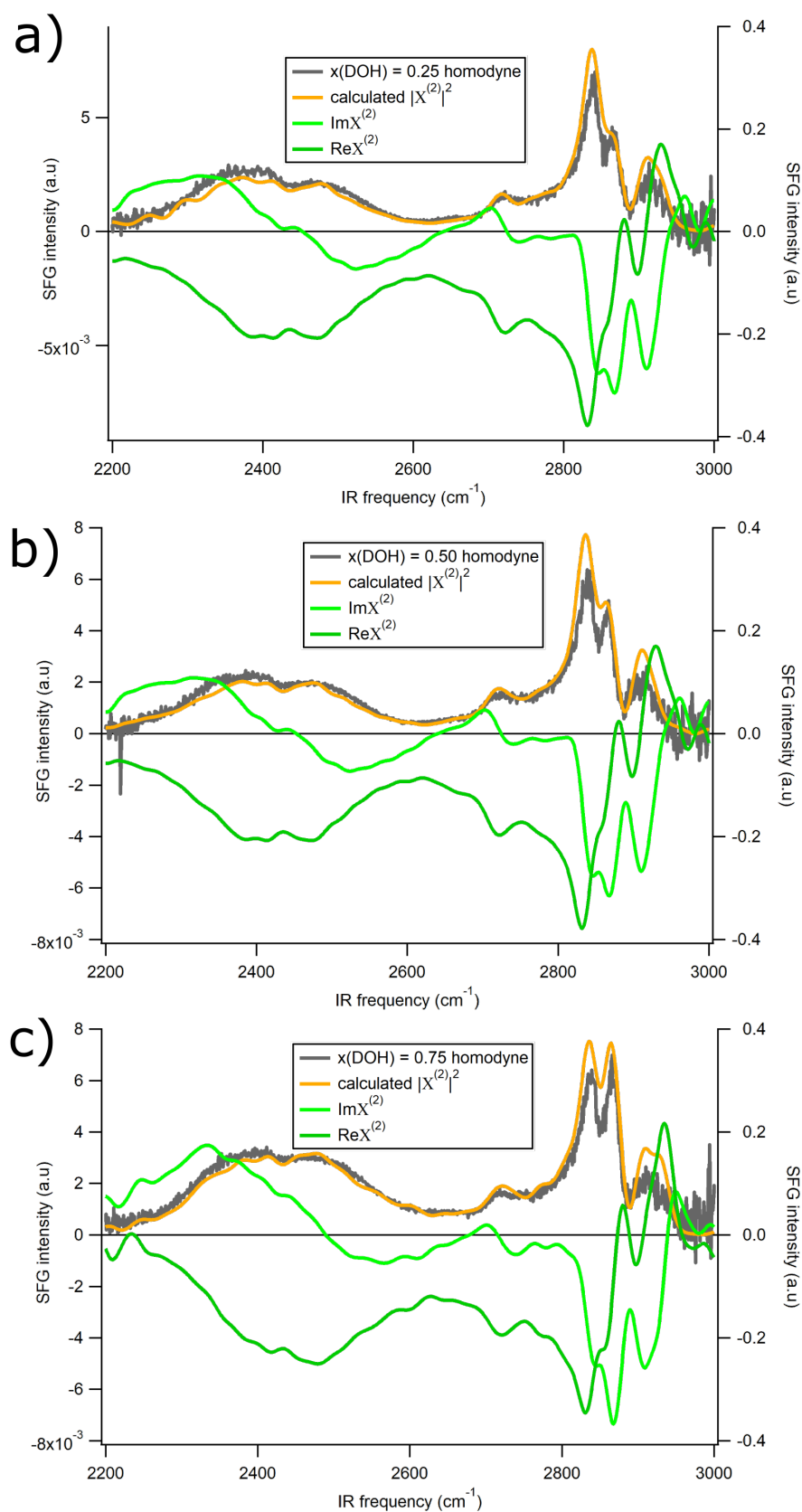


Figure 3.17: Direct and phase-sensitive SFG spectra at the D₂O-air interface of surfactant mixtures a) $x=0.25$, b) $x = 0.50$ and c) $x = 0.75$ with a total surfactant concentration $c = 2 \times 10^{-8}$ mol/mL and a pH of 11.

Chapter 4

Conclusion and Outlook

The work presented in this thesis set out to analyse effects of charge neutral surfactant mixtures on water alignment at the water-air interface. It was found that non-ionic surfactant mixtures show a similar behaviour to oppositely charged surfactant mixtures on the surface tension at the water-air interface, where the surface tension is significantly lower for mixtures than for neat surfactants. This effect for charged surfactants was attributed to synergistic adsorption of catanionic head to head complexes with a higher surface activity, than the neat surfactants. It is reasonable to assume that for the non-ionic complexes a similar phenomenon is responsible and the surfactant mixtures form hydrogen bonded complexes that adsorb to the interface. SFG spectra of the CH stretch frequency domain reveal, via the intensity ratio of the CH₂ symmetric stretching mode to the CH₃ symmetric stretching mode a higher degree of order with increasing mole fraction of dodecanol. This is also in line with the formation of hydrogen bonded head to head complexes that adsorb to the surface and increase the packing density of the mixed monolayer (see Figure 3.4). In the bonded OH/OD frequency domain an increased SFG signal from pure water was observed for all surfactant mixtures and neat surfactants. Furthermore a nonlinear trend vs. the mole fraction of dodecanol was observed, where neat surfactants have an increased SFG intensity compared to the mixtures. It was proposed that different hydrogen bonding strength of the surfactants lead to varying penetration depth into the water surface of the surfactant headgroup, which may disrupt the water structure and decrease the SFG signal.

For a better understanding of the underlying cause of the described effects of surfactant mixtures, it is necessary to examine a broader range of surfactants. Lauric acid, dodecanethiol and n-dodecylphosphonic acid are some of the candidates (see appendix for SFG spectra of lauric acid and dodecanethiol). Lauric acid and n-dodecylphosphonic acid need to be at low pH to guarantee protonation, and for dodecanthiol the procedure needs to be changed, because of the low solubility even saturated solutions exhibit no measurable surface activity. But the monolayer could still be applied with a micro syringe and a quickly evaporating dichloromethane (DCM) solution.

Spectral fitting would strengthen the results found in this thesis and eliminate problems in the analysis with effects of overlapping peaks, masking the true contributions of the vibrational modes. Furthermore the tensiometry data presented in section 3.1 have a large error and need to be refined, for a stronger argument to be made. The results could be improved by limiting the evaporation, using a lid to close of the sample from the surroundings. In the past surface pressure-area per molecule (π -A) isotherms for pure dodecanol films have been obtained using the pendent drop method (see figure 2.6).[13] This could proof useful for the dodecanol/dodecylamine mixtures and could reveal further information on the ordering and packing density of the monolayers analysed with SFG spectroscopy.

Initially experiments, where the monolayer was spread on the water surface by placing a quickly evaporating DCM solution on top, were disregarded because of concerns that, due to a much better solubility of dodecanol in water, dodecanol in a mixed monolayer could diffuse faster into the unsaturated bulk and therefore could change the composition of the monolayer over time. Decreasing SFG signal for a dodecanol monolayer spread in this manner was observed (see figure

5.7 in the appendix). Nevertheless in combination with (π -A) isotherms for all mixtures these experiments could yield useful information.

Brewster angle microscopy (BAM) could be used as a tool to monitor the homogeneity of the monolayers and to see, whether the formation of macroscopic domains could be the cause of the varying SFG signal found for the experiments using a non-rotating trough.

The SFG spectra of mixtures containing dodecylamine show NH stretch features overlapping with the bonded OH frequency domain. By using isotopically diluted water and probing the HOD bending frequency domain, the overlap with the NH_2 bending mode could be avoided. Furthermore by generally probing the HOH bending mode, contributions of dodecanol to the OH bending spectrum could be avoided, since dodecanol has no bending mode. This could help to disentangle contributions of the nonionic surfactant and of water and could lead to a better understanding of the water-surfactant-air interface.

Computational methods have proven themselves as a crucial tool for understanding interfaces in the past and could also help in understanding the effects of nonionic surfactant mixtures on water alignment. Both molecular dynamics (MD) studies as well as simulated SFG spectra could help to verify the proposed organisation of the mixed monolayers and their effect on the SFG intensity.

Chapter 5

Methods

5.1 Sample Preparation

5.1.1 H₂O dodecanol solution

The aqueous dodecanol solutions were prepared by adding $m = 3.73$ mg of dodecanol (Sigma-Aldrich) to a volume of a KOH (Sigma Aldrich) stock solution totalling an amount of substance of $n = 10^{-3}$ mol. Then purified water was added up to a total volume of one litre. The solution was then put in an ultrasonic bath for 20 minutes and 30°C. Samples had to be prepared on the same day since effects of sample degradation were observed after some time.

5.1.2 H₂O dodecylamine solution

The aqueous dodecylamine solutions were prepared by adding $m = 3.71$ mg of dodecylamine (Acros Organics) to a volume of a KOH (Sigma-Aldrich) stock solution totalling an amount of substance of $n = 10^{-3}$ mol. Then purified water was added up to a total volume of one litre. The solution was then put in an ultrasonic bath for 20 minutes and 30°C. Both solutions were mixed in a 3:1, 1:1 and 1:3 ratio for the other samples.

5.1.3 D₂O dodecanol solution

The dodecanol solutions in deuterated water were prepared by adding $m = 0.19$ mg of dodecanol (Sigma-Aldrich) to a volume of a KOH (Sigma-Aldrich) stock solution totalling an amount of substance of $n = 5 \times 10^{-5}$ mol. Then D₂O was added up to a total volume of 50 mL. The solution was then put in an ultrasonic bath for 20 minutes and 30°C.

5.1.4 D₂O dodecylamine solution

The dodecylamine solutions in deuterated water were prepared by adding $m = 0.19$ mg of dodecylamine (Acros Organics) to a volume of a KOH (Sigma-Aldrich) stock solution totalling an amount of substance of $n = 5 \times 10^{-5}$ mol. Then D₂O was added up to a total volume of 50 mL. The solution was then put in an ultrasonic bath for 20 minutes and 30°C.

5.2 Tensiometry

The surface pressure was measured using a commercial tensiometer (Kibron Inc., Finland). For the surface tension measurements the needle was first cleaned with ethanol and then heated in an open flame until red hot. Afterwards the needle was suspended from the tensiometer and then calibrated. A teflon coated aluminium trough was filled with 60 mL of Milli-Q purified water. A value of roughly -270 mV was taken for the probe in air, and a value of roughly 540 mV with the

needle in the water surface. With these two values the zero pressure for water was established. The water was measured for roughly two minutes and then the water was exchanged for the surfactant solution. The needle was lowered into the surface and as soon as a meniscus is formed the needle was pulled away two quarter rotations of the tensiometer height control wheel. The tensiometer was in a box with a closed lid and nitrogen flushing was turned on. It was measured for approximately ten minutes and then the needle was reapplied in the same manner multiple times.

5.3 Direct SFG

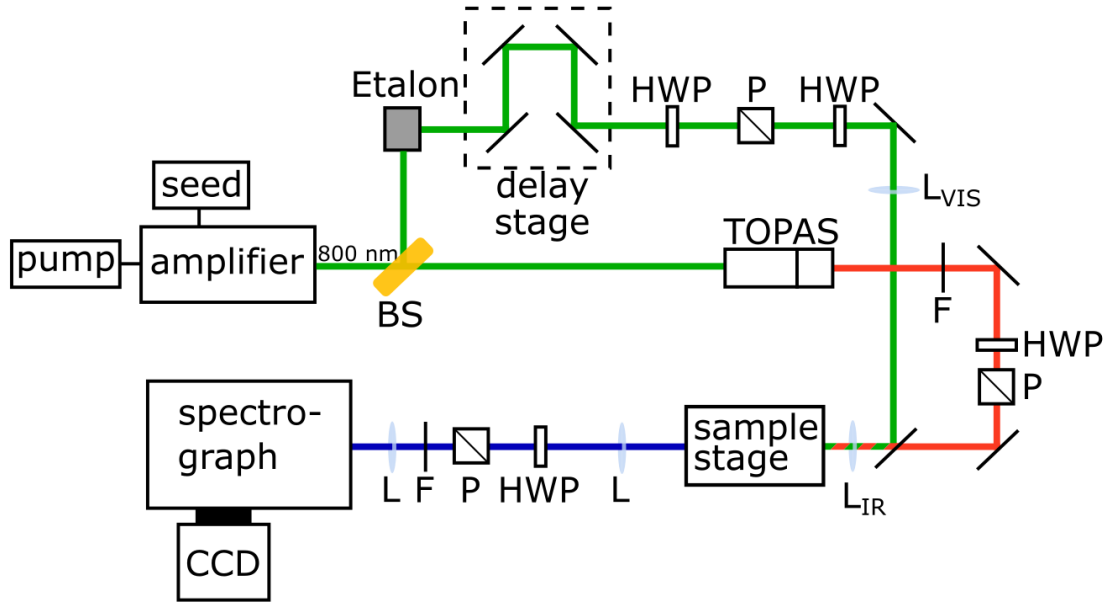


Figure 5.1: Schematic drawing of a typical direct SFG setup.[40]

Figure 5.1 shows a schematic drawing of a typical direct SFG setup. In this work, a Ti:sapphire regenerative amplifier (Spitfire Ace, Spectra-Physics) is used. The amplifier is seeded by a short mode-locked femtosecond laser pulse provided by the Mai Tai Ti:sapphire oscillator (Spectra-Physics). The seed pulse is stretched in time to not damage the Ti:sapphire crystal. To achieve a population inversion the crystal is then exited by a pump laser pulse (Empower, Spectra-Physics). The seed pulse then creates stimulated emission, creating an amplified coherent beam in the same direction and with the same energy. The Pulse is then compressed to create a pulse at 800 nm (green line in Figure 5.1 with a pulse duration of 40 fs, a repetition rate of 1 kHz and an energy of 5 mJ).

A beam splitter (BS) splits the beam, and around 1.7 mJ of the laser output are used to generate the broadband IR pulse (red line). Through optical parametric amplification in β -BaB₂O₄ crystals (TOPAS-C, Spectra-Physics) a signal and idler pulse are generated. The IR pulse is then generated by mixing both pulses in a AgGaS₂ crystal and the signal and idler pulses are filtered by a filter (F).

The other part of the beam split by the beam splitter is passed through a Fabry-Perot etalon (SLS Optics Ltd.) and generate a narrowband VIS pulse. The beam is then passed through a delay stage to temporally overlap the VIS and IR beam at the sample surface. Both beams are passed through a half-waveplate (HWP) and a polarizer (P) to control the polarization. The additional half-waveplate in the VIS beam path can be used to decrease the pulse power.

The SFG pulse generated at the sample surface are collimated with a lens (L) and then directed through a half-waveplate, a polarizer and a filter to remove reflected IR and VIS light. The pulse is then focused onto a spectrograph (Acton, Princeton Instruments) and detected by a electron-multiplied charge coupled device (CCD) (Newton, AndorInstruments).[40]

5.3.1 Experimental Procedure

In the SFG experiments a 4.5 cm diameter teflon trough was used. It was cleaned by washing with ethanol, acetone and afterwards multiple times with purified water. The trough was then set on the sample stage and 6 mL of the sample were put into the trough. In one of the setups used the rotation stage was then turned on, the other used setup did not allow for a rotation stage to be used. The box containing the sample stage was then closed off and nitrogen flushing was turned on to reduce the humidity. After about 10 minutes of flushing the first measurement was started. At the beginning and the end of each measurement cycle a z cut quartz reference was measured. To measure the background the IR beam was blocked. The samples, were measured for two times 90 s and the quartz reference was measured for two times five seconds.

5.3.2 Data Processing

For the direct SFG data, first the background was subtracted and then divided by the measuring time. Figure 5.2 shows SFG spectra that have not been normalized of quartz and a dodecanol sample with a concentration of $c = 2 \times 10^{-8}$ mol/mL. The quartz reference shows the range of the IR laser. To remove the spectral shape of the IR laser, the spectra are normalized by dividing the spectra through the quartz reference. There have been reports that an adsorbed water layer on the quartz may contaminate the spectrum, however this effect is not taken into account in this work.[3] The x-axis was calibrated previously and this axis was used.

The spectral integration was performed by subtracting a baseline, filling in the area and calculating the filled area with the vector graphics program *Inkscape*.

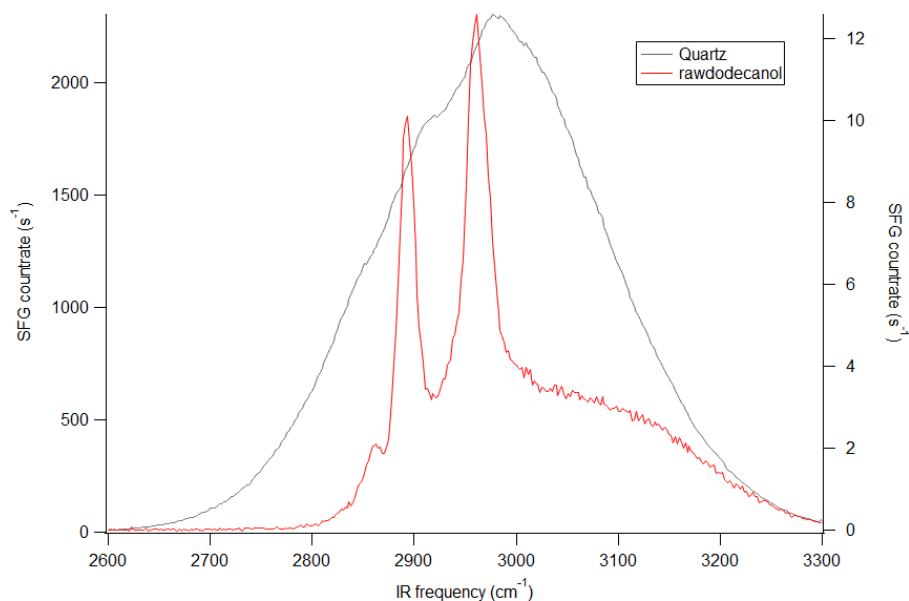


Figure 5.2: Non-normalized SFG spectra of quartz and an aqueous dodecanol solution.

5.4 Phase-sensitive SFG

For the phase-sensitive SFG measurements, H_2O and D_2O were measured in between samples for easier phase correction, since the phase of the quartz is not as stable. The phase-sensitive SFG spectra were sampled over two times 30 s. In the D_2O frequency domain nitrogen flushing is specially important because of the CO stretch vibrations of CO_2 absorb a part of the IR spectrum at around 2300 cm^{-1} .

5.4.1 Data Processing

Figure 5.3 shows the raw phase-sensitive SFG spectra of z-cut quartz, dodecanol and D_2O .

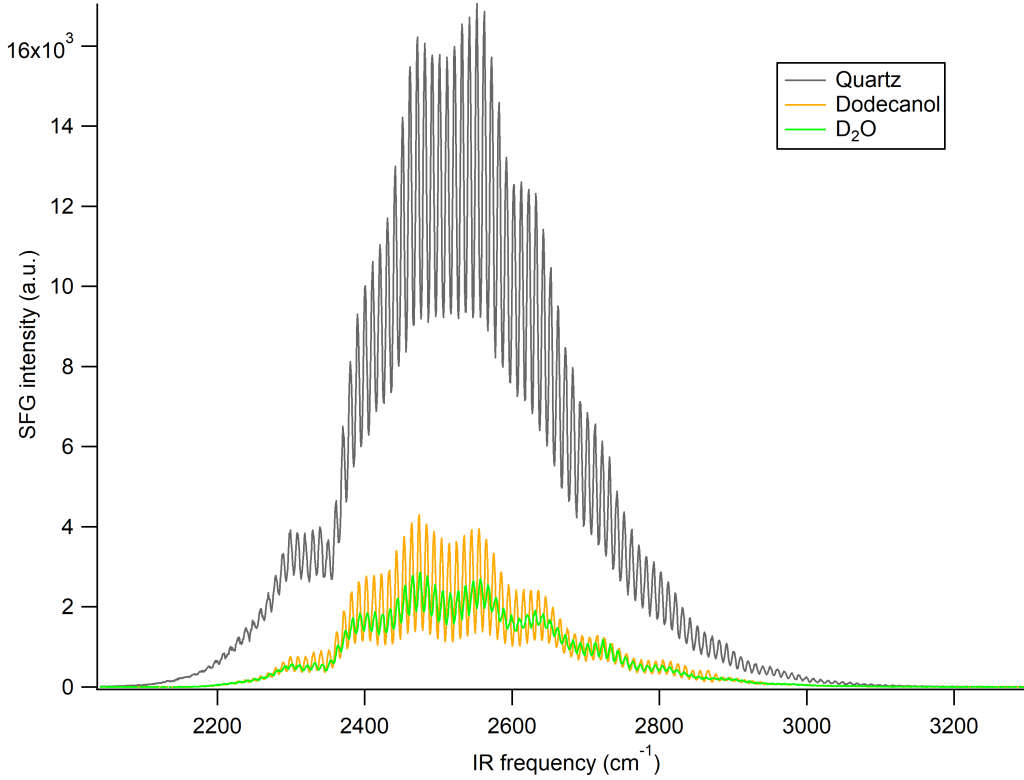


Figure 5.3: Raw phase-sensitive spectra of Quartz, dodecanol and D_2O .

Inverse fast Fourier transformation (IFFT) of the raw D_2O spectrum in figure 5.3 yields the time domain interferogram shown in figure 5.4. The peak at t_0 is due to the $|\vec{E}_{\text{sample}}|^2$ and $|\vec{E}_{\text{LO}}|^2$ terms of equation 2.38.[22] The signal at the delay time t_d , caused by the silica delay plate, can be extracted by using a window function (green line).

Fast Fourier transformation (FFT) of the filtered time interferogram yields the complex spectrum of $\vec{E}_{\text{sample}}\vec{E}_{\text{LO}}^*\exp(i\omega T)$ shown in figure 5.5 a). Dividing by the quartz reference spectrum, processed in the same manner, yields the $\chi^{(2)}$ spectrum of D_2O shown in figure 5.5 b). Figure 5.5 c) show the complex $\chi^{(2)}$ spectrum with a phase correction of 88° . The phase correction was first done for D_2O and H_2O , compared to a reference[41] and then applied to the surfactant spectra.

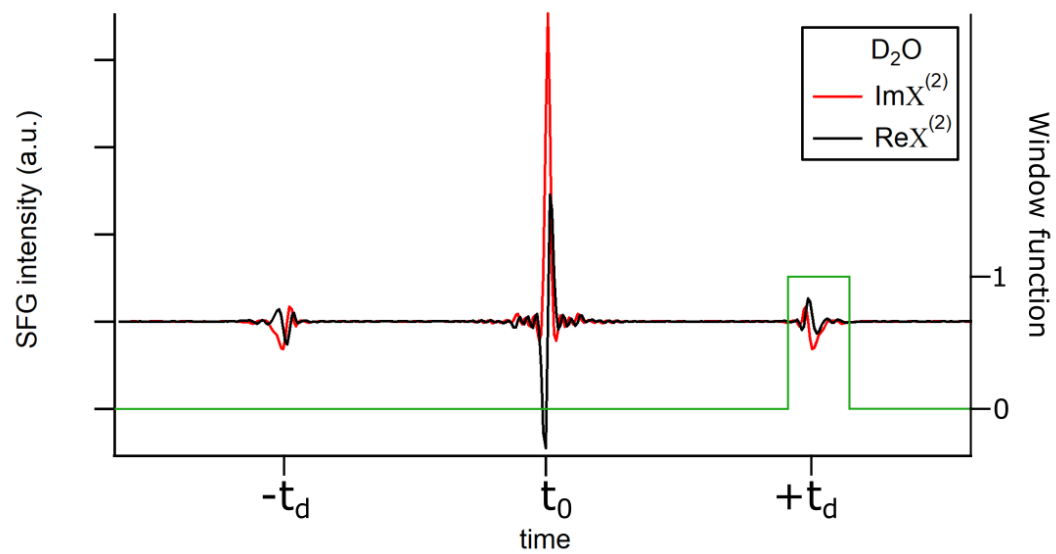


Figure 5.4: Time domain interferogram (red and black) and the window function (green).

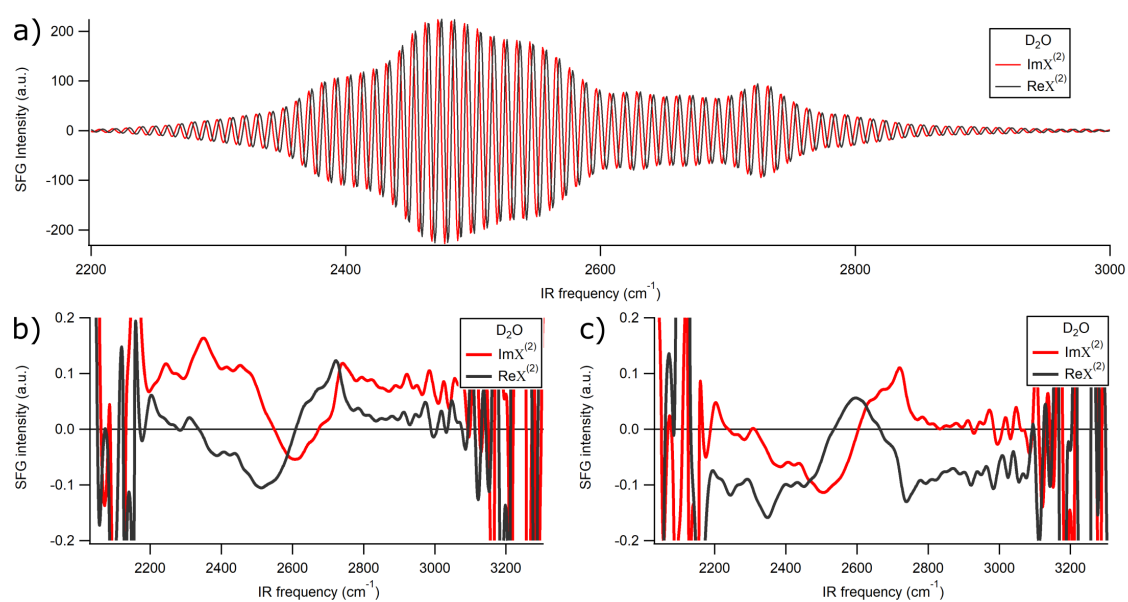


Figure 5.5: a) Real (black) and imaginary (red) part of the complex $\chi^{(2)}$ spectrum, b) normalised $\chi^{(2)}$ spectrum and c) normalised and phase corrected $\chi^{(2)}$ spectrum.

Appendix

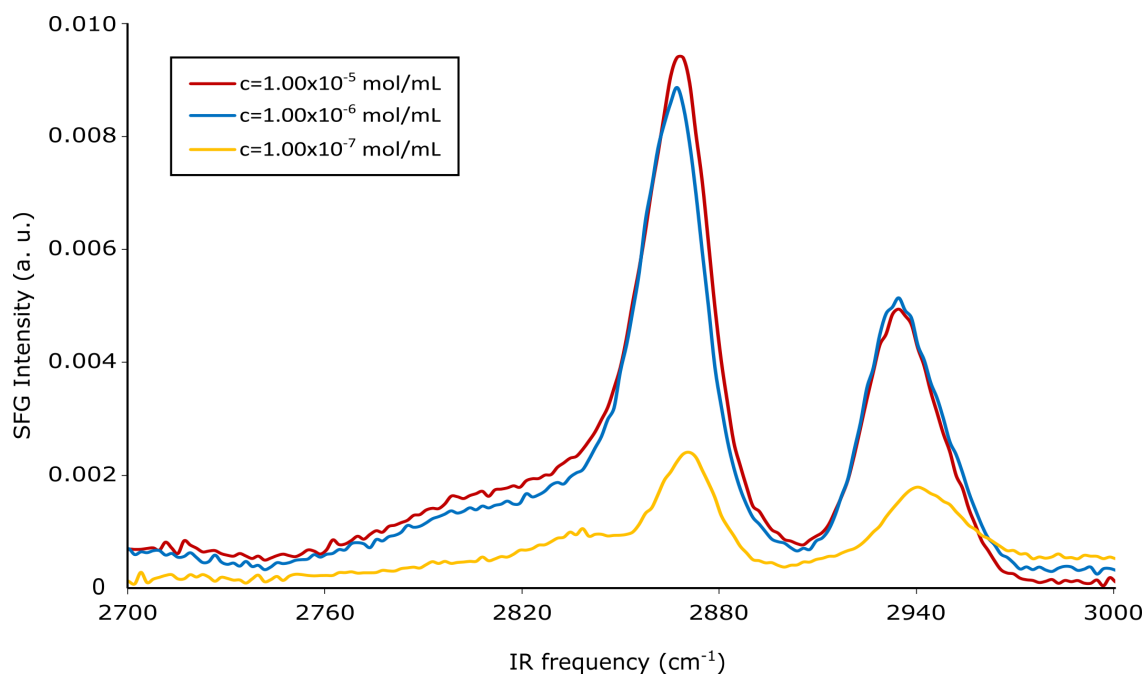


Figure 5.6: Direct SFG spectra of aqueous dodecanol solutions with different concentrations. The x-axis was not properly calibrated. For the lowest concentration the d^+ is more pronounced and the d^+/r^+ is roughly 0.5 compared to the roughly one third for the higher concentrations. This means the higher concentration monolayers are more densely packed and exhibit less gauche defects.

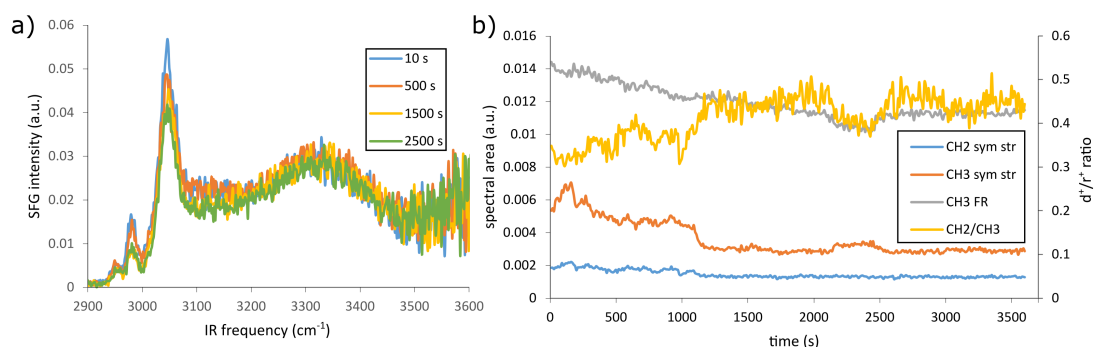


Figure 5.7: a) Dodecanol spectra after 10 s, 500 s, 1500 s and 2500 s. The monolayer was spread on a pH 11 KOH solution out via $26 \times 0.5 \mu\text{L}$ drops of a solution of dodecanol in DCM with a concentration of $c = 10^{-3} \text{ mol/mL}$. This corresponds to roughly $20 \text{ \AA}^2/\text{molecule}$. The x-axis was not properly calibrated. b) Spectral area plotted against time for d^+ , r^+ and r_{FR}^+ peaks and d^+/r^+ ratio over time. The ratio increases over time until it fluctuates around a somewhat stable level. This means that disorder increases over time. The reason could be that dodecanol molecules diffuse into the bulk and the monolayer gets less dense over time.

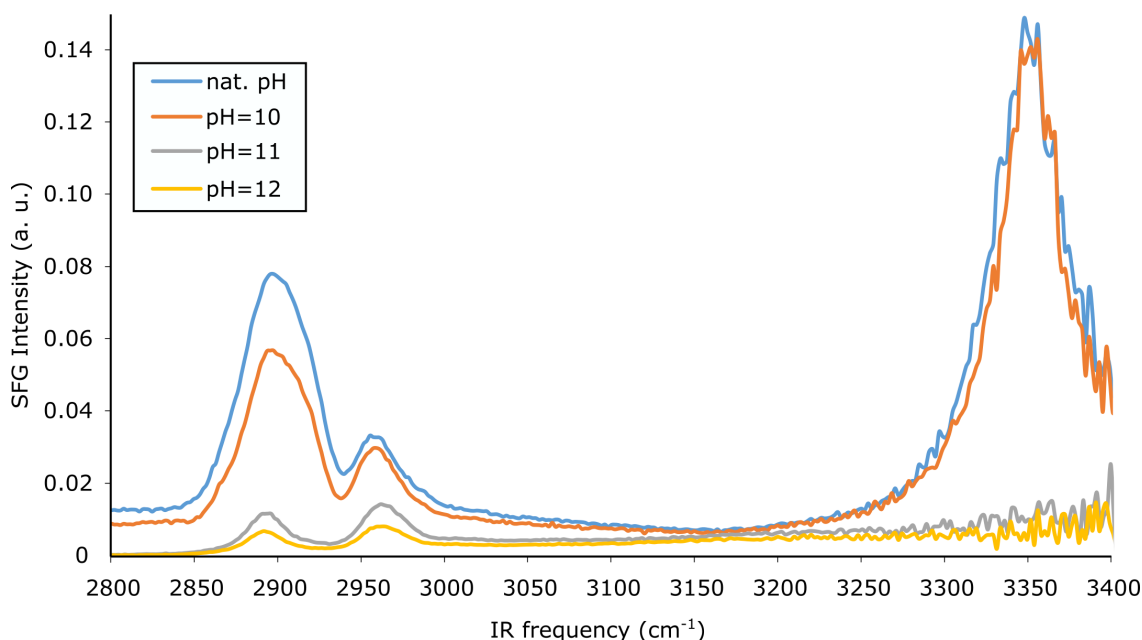


Figure 5.8: SFG spectra of oversaturated dodecylamine solutions (target concentration was $c = 10^{-5} \text{ mol/mL}$) at different pH. At natural pH and pH=10 the CH peaks have a higher intensity than at higher pH and a peak arises at 3350 cm^{-1} , which is most likely a N^+H stretch mode. The x-axis was not properly calibrated.

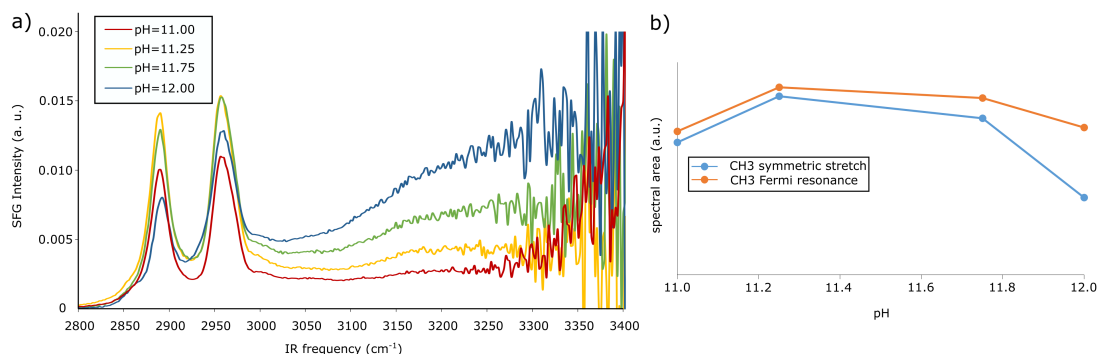


Figure 5.9: a) SFG spectra of oversaturated dodecylamine solutions (target concentration was $c=10^{-7}$ mol/mL) at different pH. At higher pH the bonded OH stretch frequency region becomes enhanced. The x-axis was not properly calibrated. b) Spectral area of the r^+ and r_{FR}^+ plotted against pH. A maximum peak area is reached for pH=11.25.

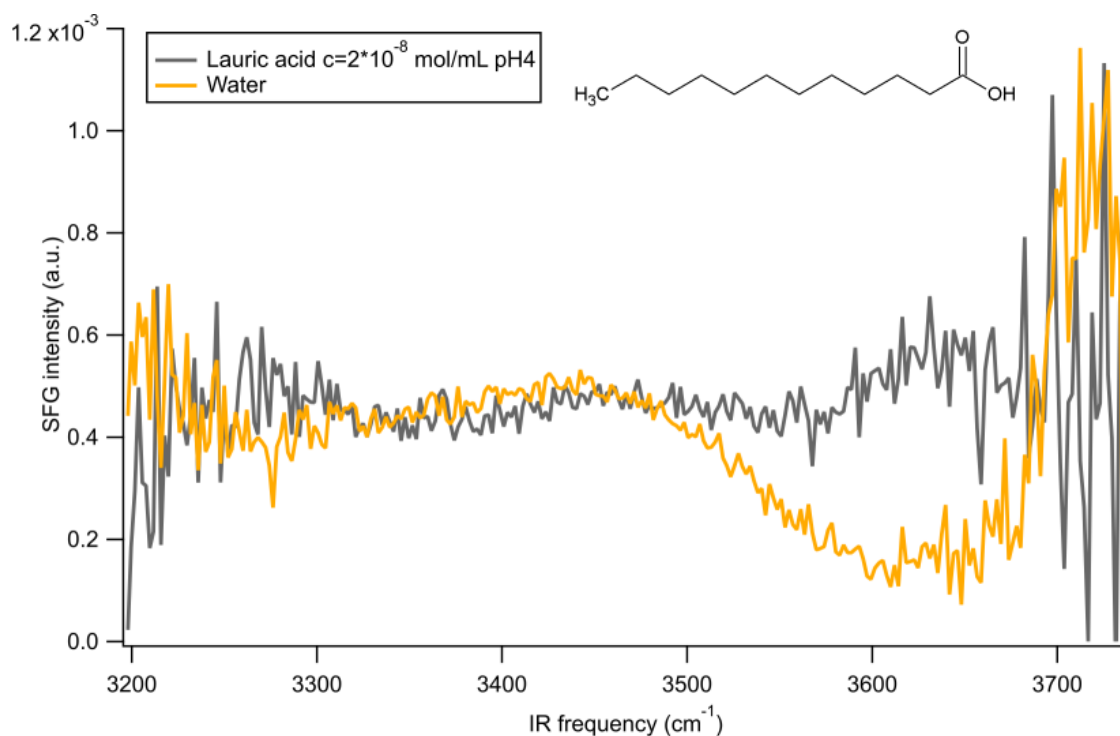


Figure 5.10: SFG spectra of an aqueous lauric acid solution with a concentration of $c=2 \times 10^{-8}$ mol/mL and a pH of 4 to ensure protonation, and neat water. The x-axis was not properly calibrated. The 3450 cm⁻¹ peak is identical for water and lauric acid solution but an additional peak at 3650 cm⁻¹ is present in the lauric acid spectrum.

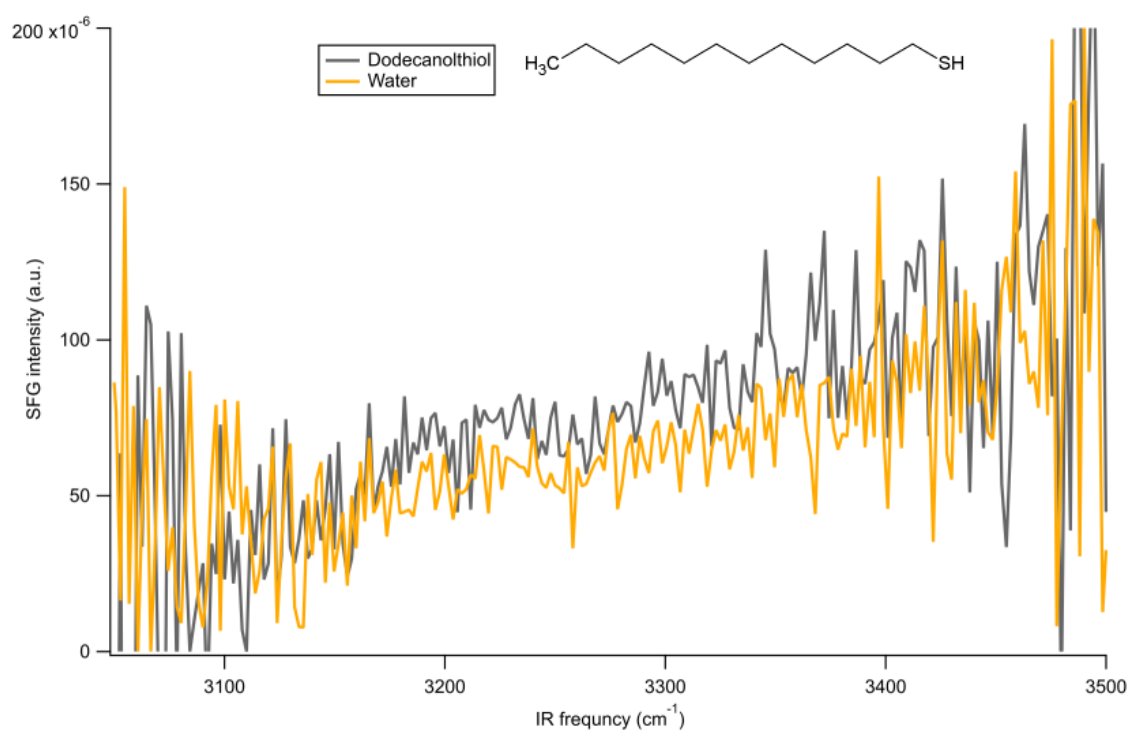


Figure 5.11: SFG spectra of neat water and an aqueous oversaturated solution of dodecanthiol (Target concentration was $c = 2 \times 10^{-8}$ mol/mL). The x-axis was not properly calibrated. The two spectra are almost identical, which means that no dodecanthiol is present at the surface. Because of the low solubility of dodecanthiol it is not suitable for the measurements of adsorbed monolayers and a monolayer would need to be spread on the surface to be analysed.

Bibliography

1. Stiopkin, I. V. *et al.* Hydrogen bonding at the water surface revealed by isotopic dilution spectroscopy. *Nature* **474**, 192–195 (2011).
2. Riedel, E. & Janiak, C. *Anorganische Chemie* 8th ed. (Walter de Gruyter GmbH & Co. KG, Berlin/New York, 2011).
3. Tang, F. *et al.* Molecular Structure and Modeling of Water-Air and Ice-Air Interfaces Monitored by Sum-Frequency Generation. *Chemical Reviews* **120**, 3633–3667 (2020).
4. Dreier, L. B. *et al.* Saturation of charge-induced water alignment at model membrane surfaces. *Science Advances* **4**, 1–8 (2018).
5. Fauser, H., Uhlig, M., Miller, R. & von Klitzing, R. Surface Adsorption of Oppositely Charged SDS:C(12)TAB Mixtures and the Relation to Foam Film Formation and Stability. *Journal of Physical Chemistry B* **119**, 12877–12886 (2015).
6. Chattoraj, D. K. & Birdi, K. S. *Adsorption and the Gibbs Surface Excess* ISBN: 978-1-4615-8333-2 (Plenum Press, New York, 1984).
7. Láng, G. G. Basic interfacial thermodynamics and related mathematical background. *Chem-Texts* **1**, 1–17 (2015).
8. Bermúdez-Salguero, C. & Gracia-Fadrique, J. Gibbs excess and the calculation of the absolute surface composition of liquid binary mixtures. *Journal of Physical Chemistry B* **119**, 5598–5608 (2015).
9. Wilhelmy, L. Ueber die Abhängigkeit der Capillaritäts-Constanten des Alkohols von Substanz und Gestalt des benetzten festen Körpers. *Annalen der Physik und Chemie* **119**, 177–217 (1863).
10. Adamson, A. W. *Physical Chemistry of Surfaces* Third Edition (John Wiley & Sons, New York, 1976).
11. Andreas, J. M., Hauser, E. A. & Tucker W. B. Boundary Tension by Pendant Drops. *Journal of Physical Chemistry* **42**, 1001–1019 (1938).
12. Padday, J. F. & Pitt, A. R. Pashley R. M. Menisci at a Free Liquid Surface: Surface Tension from the Maximum Pull on Rod. *Journal of the Chemical Society, Faraday Transactions 1: Physical Chemistry in Condensed Phases*, 1919–1931 (1975).
13. Wu, P. C., Lin, S. Y. & Tsay, R. Y. Phase transition phenomena of the adsorbed 1-dodecanol monolayer at the air–water interface. *Journal of the Chinese Institute of Chemical Engineers* **38**, 443–450 (2007).
14. Tsay, R. Y., Wu, T. F. & Lin, S. Y. Observation of G–LE and LE–LC Phase Transitions of Adsorbed 1-Dodecanol Monolayer from Dynamic Surface-Tension Profiles. *Journal of Physical Chemistry B* **108**, 18623–18629 (2004).
15. Lambert, A. G., Davies, P. B. & Neivandt, D. J. Implementing the Theory of Sum Frequency Generation Vibrational Spectroscopy: A Tutorial Review. *Applied Spectroscopy Reviews* **40**, 103–145. ISSN: 0570-4928 (2005).

16. Shen, Y. R. *Fundamentals of Sum-Frequency Spectroscopy* ISBN: 9781316162613 (Cambridge University Press, Cambridge, 2016).
17. Shen, Y. R. Surface properties probed by second-harmonic and sum-frequency generation. *Nature* **337**, 519–525 (1989).
18. Franken, P. A., Hill, A. E., Peters, C. W. & Weinreich, G. Generation of Optical Harmonics. *Physical review letters* **7** (1961).
19. Shen, Y. R. Surface probed by nonlinear optics. *Surface Science* **299-300**, 551–562 (1994).
20. Pool, R. E., Versluis, J., Backus, E. H. G. & Bonn, M. Comparative study of direct and phase-specific vibrational sum-frequency generation spectroscopy: advantages and limitations. *Journal of Physical Chemistry B* **115**, 15362–15369 (2011).
21. Ostroverkhov, V., Waychunas, G. A. & Shen, Y. R. New information on water interfacial structure revealed by phase-sensitive surface spectroscopy. *Physical review letters* **94**, 046102 (2005).
22. Nihonyanagi, S., Yamaguchi, S. & Tahara, T. Direct evidence for orientational flip-flop of water molecules at charged interfaces: a heterodyne-detected vibrational sum frequency generation study. *Journal of chemical physics* **130**, 204704 (2009).
23. Seki, T. *et al.* Decoding the molecular water structure at complex interfaces through surface-specific spectroscopy of the water bending mode. *Physical Chemistry Chemical Physics* **22**, 10934–10940 (2020).
24. Zhuang, X., Miranda, P. B., Kim, D. & Shen, Y. R. Mapping molecular orientation and conformation at interfaces by surface nonlinear optics. *Physical Review B: Condensed Matter* **59**, 12632–12640 (1999).
25. MacPhail, R. A., Strauss, H. L., Snyder, R. G. & Elliger, C. A. Carbon-hydrogen stretching modes and the structure of n-alkyl chains. 2. Long, all-trans chains. *Journal of Physical Chemistry* **88**, 334–341 (1984).
26. Sun, Q. & Guo, Y. Vibrational sum frequency generation spectroscopy of the air/water interface. *Journal of Molecular Liquids* **213**, 28–32 (2016).
27. Du, Q., Superfine, R., Freysz, E. & Shen, Y. R. Vibrational spectroscopy of water at the vapor/water interface. *Physical review letters* **70**, 2313–1316 (1993).
28. Schaefer, J., Backus, E. H. G., Nagata, Y. & Bonn, M. Both Inter- and Intramolecular Coupling of O-H Groups Determine the Vibrational Response of the Water/Air Interface. *Journal of Physical Chemistry Letters* **7**, 4591–4595 (2016).
29. Lehman, J. M. *Study of Surface Tension, Natural Evaporation, and Subcooled Boiling Evaporation of Aqueous Surfactant Solutions* Master Thesis (Embry-Riddle Aeronautical University, Daytona Beach, Florida, 2016).
30. Hu, D., Mafi, A. & Chou, K. C. Revisiting the Thermodynamics of Water Surfaces and the Effects of Surfactant Head Group. *Journal of Physical Chemistry B* **120**, 2257–2261 (2016).
31. Seffler, G. A., Du, Q., Miranda, P. B. & Shen, Y. R. Surface crystallisation of liquid n-alkanes and alcohol monolayers studied by surface vibrational spectroscopy. *Chemical Physics Letters*, 347–354 (1995).
32. Nguyen, K. T. & Nguyen, A. V. Suppressing interfacial water signals to assist the peak assignment of the N⁺-H stretching mode in sum frequency generation vibrational spectroscopy. *Physical Chemistry Chemical Physics* **17**, 28534–28538 (2015).
33. Seki, T. *et al.* Unveiling Heterogeneity of Interfacial Water through the Water Bending Mode. *Journal of Physical Chemistry Letters* **10**, 6936–6941 (2019).
34. Qurrat-ul-Ain *et al.* Anionic azo dyes removal from water using amine-functionalized cobalt-iron oxide nanoparticles: a comparative time-dependent study and structural optimization towards the removal mechanism. *RSC Advances* **10**, 1021–1041 (2020).

35. Backus, E. H. G., Bonn, D., Cantin, S., Roke, S. & Bonn, M. Laser-Heating-Induced Displacement of Surfactants on the Water Surface. *Journal of Physical Chemistry B* **116**, 2703–2712 (2012).
36. Ueta, H., Chen, L., Beck, R. D., Colón-Díaz, I. & Jackson, B. Quantum state-resolved CH₄ dissociation on Pt(111): coverage dependent barrier heights from experiment and density functional theory. *Physical Chemistry Chemical Physics* **15**, 20526–20535 (2013).
37. Stiopkin, I. V., Jayathilake, H. D., Bordenyuk, A. N. & Benderskii, A. V. Heterodyne-Detected Vibrational Sum Frequency Generation Spectroscopy. *Journal of the American Chemical Society* **130**, 2271–2275 (2008).
38. Fileti, E. E., Chaudhuri, P. & Canuto, S. Relative strength of hydrogen bond interaction in alcohol–water complexes. *Chemical Physics Letters* **400**, 494–499 (2004).
39. Roy, S., Biswas, B., Mondal, J. A. & Singh, P. C. Heterodyne-Detected Vibrational Sum Frequency Generation Study of Air–Water–Fluoroalcohol Interface: Fluorocarbon Group-Induced Structural and Orientational Change of Interfacial Water. *Journal of Physical Chemistry C* **122**, 26928–26933 (2018).
40. Dreier, L. B. *Spectroscopic Studies of Water at Charged Interfaces* Dissertation (Johannes Gutenberg-Universität Mainz, Mainz, 2018).
41. Sun, S. *et al.* Orientational Distribution of Free O-H Groups of Interfacial Water is Exponential. *Physical review letters* **121**, 246101 (2018).

List of Figures

2.1	Surfactant molecules mentioned in this work. a) Dodecanol (DOH) b) Dodecylamine (DA) c) Dodecylamine hydrochloride (DAH) d) Sodium dodecyl sulfate (SDS) e) Dodecyltrimethylammonium bromide (C ₁₂ TAB) f) Hexadecylamine (HAD).	3
2.2	Schematic drawing of the attractive forces which result in a net inward force and thus a higher potential energy for surface molecules.[6]	4
2.3	Schematic drawing of a liquid film stretched in a wireframe.[6]	4
2.4	a) Real system with the inhomogeneous surface phase AA'BB'. b) Idealized Gibbs model of the liquid column with the Gibbs dividing surface GG'.[6] [7]	5
2.5	Schematic drawing of geometry of the used tensiometer, as described by Padday and coworkers.[12]	7
2.6	The phase transition mechanism of a 1-dodecanol monolayer at the air water interface at 20 °C taken from Wu and coworkers.[13]	7
2.7	Schematic drawing of the underlying principle of vibrational sum frequency generation spectroscopy.[15]	8
2.8	Energy level diagram of the sum frequency generation process a) on and b) off resonance.[15]	9
2.9	Schematic drawing of a) a perpendicular s-polarized incident electric field \vec{E}_I and b) a parallel p-polarised incident electric field \vec{E}_I .	12
2.10	Non normalized direct and phase-sensitive SFG spectra of a) a quartz reference and b) a dodecanol monolayer on water. Both cases show deep fringes because the SFG response is comparable in magnitude to the local oscillator.	13
2.11	Geometry of the PS-SFG detection by Pool and coworkers.[20]	14
2.12	Methyl and Methylene stretch modes.[15][25]	15
2.13	Schematic energy diagram of Fermi resonance of the methyl symmetric stretch.[25]	16
2.14	Vibrational modes of water.	16
2.15	Direct and phase-sensitive SFG spectra at the D ₂ O-air interface.	18
3.1	Surface pressure measurements of mixtures of aqueous dodecanol and dodecylamine solutions with a total surfactant concentration of $c = 2 \times 10^{-8}$ mol/mL and pH 11.	20
3.2	a) Surface pressure plotted against mole fraction of dodecanol $x(\text{DOH})$. b) Surface tension measurements of SDS/C ₁₂ TAB mixtures taken from Fauser and coworkers.[5]	20
3.3	a) SFG spectra over time with different mixtures of dodecylamine and dodecanol. The total surfactant concentration is $c = 2 \times 10^{-8}$ mol/mL and is displayed as the mole fraction x of dodecanol. The coloured boxes indicate the range over which the peaks were integrated. The different mixtures are offset for better visualization and the time is indicated by the brightness of the colors used. b) d ⁺ peak area plotted against mole fraction of dodecanol. c) r ⁺ peak area plotted against mole fraction x of dodecanol. d) r _{FR} ⁺ and r ⁻ peak area plotted against mole fraction x of dodecanol. e)) d ⁺ /r ⁺ peak area ratio plotted against mole fraction x of dodecanol.	22
3.4	Schematic drawing of surfactants at the air-water interface. a)Dodecylamine b) 1:1 mixture of dodecylamine and dodecanol and c)dodecanol.	23

3.5	a) d^+ peak area plotted against time. b) r^+ peak area plotted time. c) r_{FR}^+ and r^- peak area plotted against time. d) d^+/r^+ peak area ratio plotted against time. . .	24
3.6	Total spectral area of all CH peaks plotted against a) mole fraction $x(\text{DOH})$ of dodecanol and b) time.	24
3.7	a) SFG spectrum of dodecylamine in water $c = 0.02$ mM at pH 11. b) SFG spectra of 1 mM dodecylamine hydrochloride (DAH) in water. c) SFG spectra of 0.0025 mM hexadecylamine hydrochloride (DAH) in saturated NaCl solution and 0.005 mM hexadecylamine hydrochloride (DAH) in water. Figures b) and c) was taken from Nguyen and coworkers.[32]	26
3.8	a) SFG spectra of different mixtures of dodecanol (DOH) and dodecylamine in water/KOH (pH 11) with a total surfactant concentration of 2×10^{-8} mol/mL. The coloured boxes indicate the integration range. b) Spectral area of the bonded OH region plotted against the mole fraction of dodecanol $x(\text{DOH})$. The dotted line represents a hypothetical linear trend for comparison. The reason for the differing shape of the dodecylamine spectrum is unclear.	27
3.9	Proposed effect of surfactants on the water structure. a) Pure dodecanol, b) pure dodecylamine and c) one to one mixture of dodecanol and dodecylamine.	27
3.10	a) SFG spectra with $x(\text{DOH}) = 1.00$ in D_2O in the OD/CH domain. The two series a and b are from different samples. b) SFG spectra with $x(\text{DOH}) = 0.75$ in D_2O in the OD/CH domain. c) SFG spectra with $x(\text{DOH}) = 0.50$ in D_2O in the OD/CH domain. d) SFG spectra with $x(\text{DOH}) = 0.25$ in D_2O in the OD/CH domain. e) SFG spectra with $x(\text{DOH}) = 0.00$ in D_2O in the OD/CH domain. The two series a and b are from different samples. f) Integrated spectral area of the symmetric stretch CH_2 peak (d^+) plotted against time. g) Integrated spectral area of the symmetric stretch CH_3 peak (r^+) plotted against time. h) Ratio of the d^+ and r^+ spectral area plotted against time.	29
3.11	a) SFG spectra over time with different mixtures of dodecylamine and dodecanol in D_2O at a pH of 11. The total surfactant concentration used is $c = 2 \times 10^{-8}$ mol/mL and is displayed as the mole fraction x of dodecanol. The coloured boxes indicate the range over which the peaks where integrated. b) d^+ peak area, c) r^+ peak area, d) r_{FR}^+ and r^- peak area, e) d^+/r^+ peak area ratio.	30
3.12	a) Bonded OD peak area and b) free OD peak area plotted against mole fraction $x(\text{DOH})$ of dodecanol.	31
3.13	Direct and phase-sensitive SFG spectra at the D_2O -air interface of a) dodecylamine and b) dodecanol solutions with $c = 2 \times 10^{-8}$ mol/mL and a pH of 11.	32
3.14	Schematic drawing of the orientation of water molecules and the corresponding sign in the $\text{Im}\chi^{(2)}$ spectrum.[22]	33
3.15	Schematic drawing of water molecules in the surface layer for a) pure water, b) dodecylamine hydrogen bonding to water and c) dodecanol hydrogen bonding to water.	33
3.16	a) $\text{Im}\chi^{(2)}$ spectra of different mixtures of dodecanol and dodecylamine in D_2O with a total surfactant concentration of $c = 2 \times 10^{-8}$ mol/mL and neat D_2O . The bonded OD frequency region (2200 cm^{-1} - 2600 cm^{-1}) was integrated and the positive and the negative bands were plotted separately and summed up against the mole fraction of dodecanol in b).	34
3.17	Direct and phase-sensitive SFG spectra at the D_2O -air interface of surfactant mixtures a) $x = 0.25$, b) $x = 0.50$ and c) $x = 0.75$ with a total surfactant concentration $c = 2 \times 10^{-8}$ mol/mL) and a pH of 11.	35
5.1	Schematic drawing of a typical direct SFG setup.[40]	40
5.2	Non-normalized SFG spectra of quartz and an aqueous dodecanol solution.	41
5.3	Raw phase-sensitive spectra of Quartz, dodecanol and D_2O	42
5.4	Time domain interferogram (red and black) and the window function (green). . . .	43

5.5	a) Real (black) and imaginary (red) part of the complex $\chi^{(2)}$ spectrum, b) normalised $\chi^{(2)}$ spectrum and c) normalised and phase corrected $\chi^{(2)}$ spectrum.	44
5.6	Direct SFG spectra of aqueous dodecanol solutions with different concentrations. The x-axis was not properly calibrated. For the lowest concentration the d^+ is more pronounced and the d^+/r^+ is roughly 0.5 compared to the roughly one third for the higher concentrations. This means the higher concentration monolayers are more densely packed and exhibit less gauche defects.	45
5.7	a) Dodecanol spectra after 10 s, 500 s, 1500 s and 2500 s. The monolayer was spread on a pH 11 KOH solution out via 26 x 0.5 μ L drops of a solution of dodecanol in DCM with a concentration of $c = 10^{-3}$ mol/mL. This corresponds to roughly 20 \AA^2 /molecule. The x-axis was not properly calibrated. b) Spectral area plotted against time for d^+ , r^+ and r_{FR}^+ peaks and d^+/r^+ ratio over time. The ratio increases over time until it fluctuates around a somewhat stable level. This means that disorder increases over time. The reason could be that dodecanol molecules diffuse into the bulk and the monolayer gets less dense over time.	46
5.8	SFG spectra of oversaturated dodecylamine solutions (target concentration was $c = 10^{-5}$ mol/mL) at different pH. At natural pH and pH=10 the CH peaks have a higher intensity than at higher pH and a peak arises at 3350 cm^{-1} , which is most likely a N^+H stretch mode. The x-axis was not properly calibrated.	46
5.9	a) SFG spectra of oversaturated dodecylamine solutions (target concentration was $c = 10^{-7}$ mol/mL) at different pH. At higher pH the bonded OH stretch frequency region becomes enhanced. The x-axis was not properly calibrated. b) Spectral area of the r^+ and r_{FR}^+ plotted against pH. A maximum peak area is reached for pH=11.25.	47
5.10	SFG spectra of an aqueous lauric acid solution with a concentration of $c = 2 \times 10^{-8}$ mol/mL and a pH of 4 to ensure protonation, and neat water. The x-axis was not properly calibrated. The 3450 cm^{-1} peak is identical for water and lauric acid solution but an additional peak at 3650 cm^{-1} is present in the lauric acid spectrum.	47
5.11	SFG spectra of neat water and an aqueous oversaturated solution of dodecanthiol (Target concentration was $c = 2 \times 10^{-8}$ mol/mL). The x-axis was not properly calibrated. The two spectra are almost identical, which means that no dodecanthiol is present at the surface. Because of the low solubility of dodecanthiol it is not suitable for the measurements of adsorbed monolayers and a monolayer would need to be spread on the surface to be analysed.	48

List of Tables

2.1	All possible polarization combinations and their elements of $\chi_{ijk}^{(2)}$ that contribute to the spectrum. The polarization combinations are in order SFG, VIS and IR.[15]	12
2.2	Methyl and Methylene stretch modes and their respective wavenumbers of an aliphatic chain in air.[15][25]	15
2.3	Signs of molecular susceptibilities of DAA and DDA-type water molecules.[3]	17
3.1	Peak assignment.	21
3.2	Peak assignment for dodecylamine in H ₂ O at pH 11.	25
3.3	Assignment of the CH peaks in the D ₂ O spectra.	28